Retrieval of the Sea Spray Aerosol Mode from Submicron Particle Size Distributions and Supermicron Scattering during LASIC

Jeramy L. Dedrick[1], Georges Saliba[2a], Abigail S. Williams[1], Lynn M. Russell[1], Dan Lubin[1]

[1]Scripps Institution of Oceanography, University of California, San Diego, La Jolla, California, USA
[2]Pacific Northwest National Laboratory, Richland, Washington, USA
[a]now at: California Air Resources Board, Sacramento, California, USA

Correspondence to: Lynn M. Russell (lmrussell@ucsd.edu)

Abstract. Improved quantification of sea spray aerosol concentration and size is important for determining aerosol effects on clouds and climate, though accurately capturing the size distribution of the sea spray mode remains limited by the availability of supermicron size distributions. In this work, we introduce a new approach to retrieve lognormal mode fit parameters for a sea spray aerosol mode by combining submicron size distributions with supermicron scattering measurements using a Mie inversion. Submicron size distributions were measured by an Ultra-High Sensitivity Aerosol Spectrometer (UHSAS), and supermicron scattering was taken as the difference between < 10 µm and < 1 µm 3-wavelength integrating nephelometer measurements (NEPH). This UHSAS-NEPH method was applied during background marine periods of the Department of Energy Atmospheric Radiation Measurement Layered Atlantic Smoke Interactions with Clouds (LASIC) campaign on Ascension Island (November 2016 – May 2017) when the contribution of sea spray aerosol was expected to represent a large fraction of the aerosol mass and total scattering. Lognormal sea spray modal parameters were retrieved from comparisons between nephelometer measurements and a look-up table of Mie theory-simulated scattering coefficients for low error solutions that minimized the 0.4 – 1 µm residual in the UHSAS size distribution. We evaluated the UHSAS-NEPH method with a set of clean marine measurements in the North Atlantic that included supermicron size and chemical measurements, showing that measured supermicron size distributions are needed to constrain the sea spray number concentration but mass concentration was reasonably characterized using supermicron scattering. For LASIC, the UHSAS-NEPH method retrieved sea spray mode properties for approximately 88% of background marine times when the scattering variability and total particle concentrations were low (< ± 5 Mm^{-1} and < 400 cm^{-3}, respectively), ranging from 0.6 to 1.9 µm in mass mean diameter (1.47 ± 0.17 µm), 1.1 to 3.97 in modal width (2.4 ± 0.3), and mass concentration of 0.18 to 23.0 µg m^{-3} (8.37 ± 4.1 µg m^{-3}). The measured nephelometer scattering at 3 wavelengths was found to constrain the mode width marginally at the largest particle sizes in the absence of additional size and chemical measurements for defining parameters for the Mie solutions. Comparing UHSAS-NEPH retrievals to those of a fitting algorithm applied only to the submicron UHSAS number size distribution showed that correlations between retrieved mass concentration and the available mass-based sea spray tracers (coarse scattering, wind speed, and chloride) are low when supermicron measurements are not considered. This work demonstrates the added value of

Deleted: paper

Deleted: 95%

Deleted: periods during LASIC

Deleted: when scattering variability was low and particle concentrations were typical of the clean marine boundary layer (< 400 cm^{-3})

Deleted: 6

Deleted: 1.6

Deleted: 3

Deleted: 5

Deleted: 2

Deleted: 7

Deleted: 2

Deleted: 2

Deleted: 13

Deleted: 20.7

Deleted: 6

Deleted: 6

Deleted: 3.5

Deleted: only marginally constrain the mode width

supermicron scattering measurements for retrieving reasonable sea spray mass concentrations, providing the best-available, observationally-constrained estimate of the sea spray mode properties when supermicron size distribution measurements are not available.

1 Introduction

Sea spray aerosol contributes the largest natural source of particles to the global aerosol mass budget (Lewis and Schwartz, 2004). Wind-driven breaking waves and bubble bursting at the ocean surface produce sea spray particles composed of organic components and sea salts that are injected into the atmosphere (Russell et al., 2010; O'dowd et al., 1997). Field measurements have shown that sea spray aerosol makes up 10 – 30% of the particles necessary for cloud formation, known as cloud condensation nuclei (CCN), at low supersaturations in marine regions (Modini et al., 2015; Quinn et al., 2017; Sanchez et al., 2021) and thus have important implications for modeled cloud properties and climate feedbacks (Horowitz et al., 2020). Model predictions of sea spray concentration are determined by a number of different emission parameterizations (e.g., Gong, 2003; De Leeuw et al., 2011; Salter et al., 2015), which leads to uncertainties in the sea spray mass production (2.2 – 118 10^{12} kg yr^{-1}; De Leeuw et al., 2011), the shortwave scattering direct climate effect (-2.2 – -0.15 W m^{-2}; Ayash et al., 2008), and the aerosol-cloud indirect climate effect (-2.9 – +0.3 W m^{-2}; Paulot et al., 2020).

Ambient measurements of sea spray size distributions across submicron and supermicron sizes requires merging measurements from multiple instruments, often with a differential mobility analyzer (DMA) that measures submicron sizes (10 nm to 1 µm diameter) and an aerodynamic particle sizer (APS) for coarse sizes (0.5 to 10 µm diameter) (Modini et al., 2015; Saliba et al., 2019; Quinn et al., 2017). This DMA-APS-based technique has uncertainties controlled by the limited size range, resolution, and timing of each instrument, as well as by the ambient conditions. Merging mobility and aerodynamic measurements requires varying the particle density and shifting the size distribution until there is agreement between both instruments in the overlapping diameter range (Khlystov et al., 2004) due to uncertainties in particle densities of marine aerosol (Tang et al., 1997). The generally low number concentration of sea spray aerosol at supermicron sizes also causes poor counting statistics in the largest size bins of DMAs, which impacts the range of overlap to which the retrieval is sensitive (Russell et al., 1996a; Russell et al., 1996b).

Coarse mode sea spray has been retrieved using automated routines that fit a region of the merged size distribution, typically defined as particles larger than 0.4 µm diameter (0.4 – 10 µm), using a single lognormal mode (Saliba et al., 2019; Quinn et al., 2017). This diameter range often appears as a partial peak or "shoulder" in measured number and mass size distributions and is largely composed of sea salt particles during marine conditions (Quinn et al., 2017; Saliba et al., 2019; Zheng et al., 2018; Sanchez et al., 2021; Murphy et al., 1998). Lognormal fitting routines use parameters defining the shape of the mode

Deleted: The approach for this task is the combination of sizing instruments that resolve the aerosol size distribution across sub- and supermicron diameters typically

Deleted: for

(number concentration, geometric mean diameter, and geometric standard deviation) with observation-based constraints for the parameters (Modini et al., 2015; Quinn et al., 2017; Hussein et al., 2005) or as an unconstrained approach with parameters that vary freely (Saliba et al., 2019; Sanchez et al., 2021). Correlations of the single lognormal mode to wind speed and sea salt mass concentration provide justification for identifying the coarse mode as the "sea spray mode" during clean marine conditions (Saliba et al., 2019; Modini et al., 2015; Quinn et al., 2017; Lewis and Schwartz, 2004). When DMA and supermicron size distribution measurements were not available, submicron size-resolved measurements from the Ultra-High Sensitivity Aerosol Spectrometer (UHSAS) have been used for UHSAS-only retrieval of the sea spray mode (Sanchez et al., 2021; Zheng et al., 2018; Zheng et al., 2021). These methods have provided some demonstrated skill in predicting the number and cloud forming properties of sea spray particles less than 1 µm, but may not be sufficient to adequately characterize the mass concentration and optical properties of the supermicron fraction of sea spray (Murphy et al., 1998; Chamaillard et al., 2006; Kleefeld et al., 2002; O'dowd et al., 2010).

Given the uncertainties associated with merging of multiple instrument size distributions and the limited availability of supermicron size distribution measurements in marine regions, alternative methods should be considered to adequately characterize the modal properties of sea spray aerosol. Supermicron scattering measurements from nephelometers are commonly included as part of long-term atmospheric observations (Uin et al., 2019; Schmale et al., 2022) and provide an attractive alternative to supermicron size distribution measurements for constraining coarse sea spray properties (Demott et al., 2016; Testa et al., 2021). The premise of the approach proposed here is the observation that sea spray particle mass concentration often correlates to the supermicron scattering during clean marine conditions (Kleefeld et al., 2002; Chamaillard et al., 2006; Quinn et al., 1998; O'dowd et al., 2010). Scattering measurements can be translated to equivalent size distributions by employing Mie theory (Mie, 1908) using an Inverse Mie Method (IMM) with assumptions of particle size, composition, and concentration for optical properties of the particle population (Bluvshtein et al., 2017). Similar approaches that combine observed or simulated size distributions with scattering measurements have found that optical properties alone, without the addition of a particle sizer, are not sufficient to estimate properties of the aerosol size distribution (Frie and Bahreini, 2021; Shen et al., 2019; Lv et al., 2018).

In this work, we retrieved sea spray aerosol modal properties by fitting a single lognormal mode constrained by supermicron scattering at 3 wavelengths from a nephelometer to measured mass size distributions from an Ultra-High Sensitivity Aerosol Spectrometer, known here as the UHSAS-NEPH method. Since sea spray aerosol concentrations are most relevant to CCN in "clean" marine environments (Quinn et al., 2017) and the addition of non-marine sources (e.g. dust) tend to mask supermicron sea spray contributions, we directed the method at measurements that are largely reflective of clean marine conditions on Ascension Island during the Layered Atlantic Smoke Interactions with Clouds (LASIC) campaign. LASIC measurements provide an example where the sea spray size distribution needs to be retrieved, but no supermicron size distributions were measured. For comparison and support of UHSAS-NEPH with previously developed techniques, the method was also applied

Deleted: . Scattering-constrained lognormal modes that are fit to the measured size distribution are referenced from a look-up table of Mie theory-simulated scattering coefficients using a combination of fitting parameters that define the concentration, mean size, and width of the sea spray mode. Employing look-up tables in optical measurement inversions has been demonstrated in previous inversion procedures (e.g. (Lv et al., 2018; Veselovskii et al., 2002)) and is based on minimizing error between measurement and reference values for each retrieval to obtain a single solution. Recognizing the inherent restrictions of solely minimizing error to derive a single, unique solution, namely the uncertainties in comparing theory estimates and measurements, we incorporate known instrument error and measurement variability into the retrieval methodology. Within averaging intervals, uncertainty and variability have been shown to impact the assumed size distributions and optical properties of aerosol using inversion techniques (Viskari et al., 2012; Frie and Bahreini, 2021). This scheme enables a variety of solutions to be aggregated and assessed so that a consistent and unique solution can be obtained by averaging solutions that are the most statistically probable.

Deleted: at

Deleted: a location that lacked supermicron size distribution measurements

to an additional dataset that included nephelometer and submicron size measurements as well as size-resolved sea salt mass concentration and supermicron size distributions for the validation of reasonable sea spray mass retrieval.

Deleted: . This study first describes the measurements utilized for sea spray mode retrieval, followed by a summary of the method employed to quantify modal properties from these measurements. Retrieved sea spray mode properties are then compared with a submicron-only fitting algorithm, known sea spray tracers (supermicron scattering, wind speed, and chloride), and literature-reported values to evaluate the extent to which the retrieved mode is largely from sea spray. ¶

2. Measurements

2.1 LASIC

Measurements from the Department of Energy Atmospheric Radiation Measurement (DOE ARM) site on Ascension Island, Saint Helena (7.96696° S, 14.34981° W) during the Layered Atlantic Smoke Interactions with Clouds (LASIC) campaign are used to develop the sea spray mode retrieval. LASIC captured the annual and seasonal cycles of aerosol and cloud properties during an 18-month (April 2016 – October 2017) deployment of the ARM Mobile Facility 1 (AMF1) (Miller et al., 2016; Zuidema et al., 2016). AMF1 measurements were collected at an isolated site on the windward flank of Green Mountain, away from the island's airport and other inhabited areas (Zhang and Zuidema, 2019). The prevailing wind direction measured by meteorological instrumentation during the campaign was 115 ± 10° (east-southeasterly), indicating persistent sampling of offshore maritime air. The ARM Mobile Aerosol Observing System, a component of AMF1, housed the instruments, described in the following subsections, from an inlet situated 10 m above ground level at an altitude of 365 m above sea level (Uin et al., 2019).

Deleted: demonstrate the performance of the

Deleted: (MAOS)

Episodic intrusions of airborne biomass burning particles are carried into the Ascension Island marine boundary layer from South African wildfires annually during June – October (Zuidema et al., 2016). These events contrast sharply with the clean boundary layer that persists for the remainder of the year (November – May; Pennypacker et al., 2020). Non-marine aerosol particles are limited during this "background" season, though a few transport events of African dust that entrain into the boundary layer have been documented as occurring during austral summer and fall months (January – April) in the Southeast Atlantic (Kishcha et al., 2015; Virkkula et al., 2006). For background (non-biomass burning) times without dust events, the aerosol population is expected to be largely from marine sources, of which sea spray represent a large fraction of the aerosol mass concentration. This work will focus on LASIC background season observations (November 2016 – May 2017) (Table 1).

2.1.1 Submicron Particle Size Distributions

Two particle sizing instruments were operated during the LASIC campaign: a TSI Scanning Mobility Particle Sizer (SMPS; TSI Inc., Shoreview, MN, USA) and an Ultra-High Sensitivity Aerosol Spectrometer (UHSAS; Droplet Measurement Techniques (DMT) Inc., Longmont, CO, USA). The SMPS measured the aerosol size distribution ranging from 10 nm to 460 nm dry mobility diameter, which did not have sufficient overlap with the > 0.4 μm diameter range relevant for retrieving the sea spray mode (Fig. 1), meaning that it did not provide constraints on the sea spray mode retrieval and was not used here.

The UHSAS operated with 99 size channels at logarithmic spacing to cover diameters from 60 nm to 1 µm optical diameter at a temporal resolution of 1 Hz that were averaged to 1 min. The UHSAS was calibrated using polystyrene latex spheres with refractive index of approximately 1.59 and has a particle counting efficiency of approximately 100% for particle concentrations below 3000 cm^{-3} and sizes larger than 0.1 µm (Cai et al., 2008). The counts of particles per bin were converted to number size distributions using the sample flow rate (typically 50 cm^3 min^{-1}) and the sample accumulation time (10 s). UHSAS sample line relative humidity (RH) was not recorded during LASIC, so the RH of UHSAS size distribution measurements was estimated using the UHSAS internal temperature along with ambient temperature and relative humidity from the Mobile Aerosol Observing System meteorological instrumentation. The UHSAS RH was found to be 55 ± 8% during LASIC.

Deleted: dry

UHSAS artifacts at large size bins have been reported for measurements in marine air masses (Pennypacker and Wood, 2017; Sanchez et al., 2021). These artifacts appear as two consistent and narrow modes at optical particle diameters of 0.6 and 0.85 µm, which likely represent the splitting of the sea spray mode by partial drying of salt that has been sampled from high ambient relative humidity (Fig. 2). These two modes constitute low contributions to the particle number concentration (Fig. 2a), but an appreciable amount to the mass concentration (Fig. 2b) of the measured size distributions. We expect that the 0.6 µm mode is the dried part of the salt mode, similar to distributions reported by Sanchez et al. (2021), while the narrow 0.85 µm mode is the remainder of the salt mode that is only partially dried. A treatment for these artifacts to fit the sea spray mode is described in Section 3.4.

Deleted: dry

2.1.2 Supermicron Scattering

1 min averaged scattering coefficients (b_{sca}) were measured by a TSI 3563 3-wavelength integrating nephelometer at red (700 nm), green (550 nm), and blue (450 nm) light wavelengths over an angular integration range of 7° to 170° (Anderson et al., 1996) and impactor size cuts of 1 and 10 µm that alternated at intervals of about 1 h. 2-h averages of the scattering measurements for each impactor size cut were used to derive supermicron scattering coefficients at each wavelength ($b_{sca,1\text{-}10\mu m}(\lambda)$) by differencing the b_{sca} at 1 µm from b_{sca} at 10 µm. Scattering coefficients were corrected to account for known truncation errors due to significant coarse sea salt particle forward scattering at angles less than 7° (Anderson and Ogren, 1998). The detection limit of the nephelometer for typical operating conditions is between 0.1 and 0.3 Mm^{-1} depending on the wavelength (Anderson et al., 1996).

Deleted: dry

Particle scattering measurements during LASIC were not available at standard dry conditions (< 40%) as operating conditions only allowed for limited heating, typically producing 60 ± 4% RH at the nephelometer inlet for ambient conditions of 88 ± 8% RH. This average RH of 60% means particles were not dried to the efflorescence point for sea salt mixtures (< 40%) (Ming and Russell, 2001). The supermicron scattering (at 450 nm) did not show a significant correlation to the instrument RH ($R = 0.22$, $p = 0.19$; Fig. S1), but the correlation increases to $R = 0.36$ ($p < 0.05$) for RH > 60 %, indicating that at higher RH the

scattering may need to be corrected for humidity. Measurements of particle scattering at a series of pre-set RH were also collected during LASIC to provide hygroscopic growth factors (*f(RH)*) to correct scattering from 65% RH to the heated conditions (Zieger et al., 2010; Gasso et al., 2000). However, because the uncertainty for f(65% RH) was estimated to be > 30%, which was approximately fourfold greater than the 8% for < 1 µm and 7% for < 10 µm scattering uncertainties for the heated measurements, we did not apply this correction. This uncertainty was driven by the limited and non-overlapping times for which f(65% RH) was available for < 1 µm and < 10 µm scattering, each typically spanning only 30 ± 5% of the 2-h averaging period. Without sufficient and simultaneous f(RH) measurements of the humidity dependence of scattering, and given the additional uncertainties associated with correcting optical size distribution measurements with humidity and composition dependent refractive indices (Kassianov et al., 2015), correcting the measurements to a standard RH was also not possible. Instead, we restricted the measurements to include only those for which the average nephelometer humidity matched the average UHSAS RH. Restricting nephelometer measurements to those that had RH below 60% gives an average RH of 55% with 10% measurement uncertainty (55 ± 10%), while still retaining 78% of the measurements for this analysis.

2-h supermicron scattering during the LASIC background season had an average value of 12.0 ± 6.3 Mm^{-1} (0.3 – 41.1 Mm^{-1}) as measured by the nephelometer at 550 nm and made up 70 ± 7% of the total scattering for particles less than 10 µm diameter. The combined use of the submicron particle size distribution from UHSAS and the supermicron scattering coefficients from the nephelometer provide the basis for naming this method UHSAS-NEPH.

2.1.3 Uncertainty and Variability of the Size Distributions and Scattering Measurements

Measurement variability and instrument error are incorporated into the sea spray mode retrieval to account for uncertainties in the Mie theory-based inversion of scattering and size distribution measurements (Table 2; Section 3).

UHSAS sizing uncertainty is within 2.5% of the particle size (Uin, 2016) with variations of -10% to +4% based on calibrated particles with known refractive index between 1.44 and 1.58 (Moore et al., 2021). The reported systematic uncertainty of number size concentration for accumulation mode (0.1 – 1 µm) particles measured by UHSAS has been shown to be 3.9% due to calibration, flow, and pressure biases (Kupc et al., 2018). This instrument error propagates to -27.5% to +12.4% for higher moments of the size distribution such as surface area and volume (Kupc et al., 2018; Brock et al., 2019). We therefore adopt a size uncertainty value (σ_D) of 2.5% as defined by the UHSAS instrument manufacturer (Uin, 2016) and 10% for the concentration uncertainty (σ_{PNSD}) that has been used in previous inversion procedures (Bluvshtein et al., 2017; Frie and Bahreini, 2021). Measured size distribution variability was calculated for the UHSAS size distribution at each diameter bin ($\sigma_{PNSD,meas}(D_p)$) as the standard deviation of the 2-h averages.

Systematic uncertainties of the particle scattering are mainly due to non-idealities at each measurement wavelength and angular sensitivities of the nephelometer (Anderson and Ogren, 1998). These features promote the use of a scattering uncertainty ($\sigma_{sca,inst}(\lambda)$) value of 5% that has been used in previous inversion procedures (Frie and Bahreini, 2021; Bluvshtein et al., 2017). Measured scattering variability was calculated for the supermicron scattering at each wavelength ($\sigma_{sca,1\text{-}10\mu m}(\lambda)$) as the standard deviation during the 2-h average. A list of the measured size distribution and scattering variables and their associated uncertainties and variabilities are provided in Table 2. Particle losses due to aspiration and transmission in the ARM Mobile Aerosol Observing System were assessed using the particle loss calculator (PLC; Von Der Weiden et al., 2009), sample line configurations and geometry from Bullard et al. (2017), and a particle density of 1 g cm^{-3}. Losses were found to be less than 10% for particles smaller than 1 µm diameter and greater than 50% for particles larger than approximately 6 µm. We did not correct UHSAS size distributions for these losses given the uncertainty of that correction, but note that nephelometer supermicron scattering measurements may underestimate retrieved sea spray number and mass concentrations at the largest diameters. Using the mean sea spray mode statistics of UHSAS-NEPH, the particle losses in the instruments can equate to an underestimation of roughly 13 ± 8% in the sea spray mass and 0.8 ± 4% in number using nephelometer scattering.

Deleted: MAOS

2.1.4 Ancillary Variables

As an alternative to size-resolved filter measurements of sodium, which were not collected during LASIC, measurements from an aerosol chemical speciation monitor (ACSM; Aerodyne Research, Billerica, MA USA) were used to evaluate sea salt mass retrievals. ACSM provided mass and chemical composition (organics, sulfate, nitrate, ammonium, and chloride) of non-refractory submicron aerosols. Since sea salt does not volatilize efficiently at 600°C, the ACSM measurement of non-refractory chloride provides a trace signal from NaCl that is detectable in the absence of large sources of non-refractory chloride (Frossard et al., 2014; Ovadnevaite et al., 2012) and has been used as a tracer to identify sea salt aerosol contributions to CCN (Humphries et al., 2021). We use chloride measurements only for January 2017 through May 2017, as these data were quality assured. 2-h averaged ACSM chloride concentration showed statistically significant ($p < 0.05$) positive correlation with two common sea spray tracers: wind speed (R = 0.2) and nephelometer supermicron scattering at 550 nm (R = 0.33) (Fig. S2). This observation supports the potential of LASIC ACSM chloride measurements to serve as a chemical tracer for sea spray mass in the evaluation of UHSAS-NEPH.

Deleted: 1

Deleted:

Deleted: our proposed retrieval method

We additionally incorporated measurements of 1 min averaged condensation nuclei concentrations above 3 nm (CN_3) from a TSI Ultrafine Condensation Particle Counter (CPC) 3776, wind speed and rain intensity from a Vaisala WXT-520, refractory black carbon (rBC) concentration from a DMT Single Particle Soot Photometer, 470 nm particle absorption from a Radiance Research Particle Soot Absorption Photometer (PSAP), and carbon monoxide (CO) mixing ratio from a Los Gatos Research trace gas analyzer (Miller et al., 2016). These measurements were used to identify clean marine periods (Section 2.2), assess

Deleted: and to

environmental influence on retrieval performance, and evaluate the retrieved sea spray masses. Ancillary measurements were averaged to 2-h resolution to match the timing of the supermicron scattering coefficients and size distribution averages.

2.2 Measurement Screening

Non-marine aerosol particles, specifically those from combustion sources, have been shown to influence the performance of sea spray mode retrievals by contributing number and mass concentrations that overlap with the region used to fit a mode in ambient size distributions (Modini et al., 2015; Saliba et al., 2019). Here we focus on periods when boundary layer air masses are assumed to have a multi-day marine history in order to reduce non-marine sources and ensure retrieval results that are consistent with sea spray. In the case of LASIC observations, boundary layer intrusions of biomass burning aerosol can affect particle optical properties by increasing absorption and reducing scattering for sub- and supermicron particles (Delene and Ogren, 2002; Denjean et al., 2020). In particular, UHSAS instruments show under-sizing of particles when highly absorbing biomass burning aerosol are introduced into the particle population due to heating from the instrument beam and subsequent particle vaporization and shrinkage (Howell et al., 2021). Although this effect is more likely to impact particles smaller than the assumed sea spray size ($D_p \leq 0.4$ µm), any impact on potential submicron sea spray aerosol contributions would have an influence on the sea spray mode retrievals. To limit non-marine influences on UHSAS-NEPH retrieval, we first isolated measurements during "clean marine" periods of the LASIC background season from November 2016 through May 2017 by applying the following criteria (Fig. 3):

(1) CN_3 concentration less than 600 cm^{-3}, which was the approximate 90th percentile particle concentration during the LASIC campaign,

(2) CO mixing ratio (a proxy for continentally-sourced air) below the limit of ambient marine boundary layer background levels observed during LASIC (70 ppbv; Pennypacker et al., 2020),

(3) rBC concentration below the combustion source threshold of 50 ng m^{-3} used by Saliba et al. (2020) in the remote marine North Atlantic, and

(4) < 10 µm Scattering Angstrom Exponent (SAE_{10}) values less than 1 for 450 and 700 nm nephelometer scattering. SAE_{10} characterizes the wavelength dependence of particles and takes on small (< 1) values during periods in which coarse aerosol, such as sea salt, have a large mass contribution (Shen et al., 2019; Mulcahy et al., 2009).

Saharan dust and continental aerosol transport from southern Central Africa into the remote tropical Atlantic boundary layer has been a commonly observed contributor to the surface-level aerosol population at Ascension Island (Swap et al., 1996). The mass concentration of transported dust particles are largely in the supermicron size range (Miller et al., 2021; Denjean et al., 2016) and overlap the fitting region used in UHSAS-NEPH. To exclude interference in the retrieval from dust particles, we used measurements of the sub-10 µm single-scattering albedo at 470 nm (SSA_{470nm}) from NEPH scattering and PSAP absorption to identify times with possible dust influence (SI Text 1). An SSA_{470nm} threshold of 0.95 was used to distinguish

Deleted: Clean Marine Periods

Deleted: sea spray mode fitting region

Deleted: seasons

Deleted: or dust

Deleted: our

Deleted: Additionally, dust and other continental aerosol can be advected from southern central Africa and into the Southeast Atlantic marine boundary layer and affect the size overlap of the fitting region used in the UHSAS-NEPH algorithm (0.4 – 1 µm) due to increased contributions of non-sea salt coarse mode particles in the size distribution (Miller et al., 2021).

Deleted: these

Deleted: 0.07 ppb;

between sea salt and dust aerosol contributions to coarse scattering based on the relationship of SAE_{10} and average SSA reported for Saharan dust (Di Biagio et al., 2019; Von Hoyningen-Huene et al., 2009; Haywood et al., 2003). This restriction removed 68 2-h periods.

We additionally removed periods when the rain intensity exceeded 1 mm h^{-1} at any hour during the 2-h average to ensure minimal influence of precipitation on the retrieval, namely wet scavenging of sea spray aerosol by rain droplets. 14 periods exceeded this rain intensity restriction. The combination of all criteria identified 909 2-h (non-raining) clean marine periods, which accounted for approximately 40% of all available background season observations. The clean marine criteria reduced the average criteria values by 12% for CN_3, 7% for CO, 70% for rBC, and 15% for SAE_{10} after applying these restrictions. The 909 available periods provided persistent marine conditions that were low in aerosol concentration (300 ± 90 cm^{-3}) and in combustion influence (15.7 ± 12.7 ng m^{-3}), as well as having a large scattering contribution from coarse particles (SAE_{10} = 0.66 ± 0.15).

Deleted: 1240

Deleted: 50

Deleted: (Fig. 3)

Deleted: 1240

3 Sea Spray Mode Retrieval (UHSAS-NEPH)

This section outlines the procedure used to retrieve sea spray modes from scattering measurements and submicron mass size distributions (Fig. 4). We describe the relationship of particle scattering to particle size (Section 3.1) and how this theoretical relationship is used to identify a group of probable sea spray mode solutions that are consistent with the measured supermicron scattering, as well as with literature reported ranges of modal properties (Section 3.2). Mode solutions are then constrained with measured submicron mass size distributions (D_p > 0.4 µm) to isolate and retrieve the most consistent sea spray modal properties (Sections 3.3 – 3.4).

Deleted: (0.4 – 1 µm)

3.1 Simulating Sea Spray Mode Scattering using Mie Theory

A look-up table of scattering coefficients was developed by employing a modified Mie theory code based on the algorithm for red (700 nm), green (550 nm), and blue (450 nm) wavelengths (Bohren and Huffman, 1998; Mätzler, 2002). These wavelengths were chosen to match those used by the 3-wavelength integrating nephelometer operated during LASIC (Section 2.1.2). Each of the three red, green, blue (RGB) scattering coefficients is attributed to a combination of lognormal mode fitting parameters (N_t, D_g, and σ_g) that describe the shape of the sea spray mode. We use the canonical lognormal mode form to represent the number size distribution of sea spray aerosol with the following equation (Seinfeld and Pandis, 2006):

Deleted: Eq. (1)

$$\frac{dN}{dlogD_p} = \frac{N_t}{\sqrt{2\pi}\log_{10}\sigma_g} e^{-\frac{(\log_{10}D_p - \log_{10}D_g)^2}{2(\log_{10}\sigma_g)^2}} \quad (1),$$

where N_t is the number concentration of particles (cm^{-3}), D_p is the particle diameter (µm), D_g is the geometric mean diameter (µm), and σ_g is the geometric standard deviation (or mode width; unitless). These values are 1 – 99 cm^{-3} for number concentration, 0.05 – 1.19 µm for mean diameter, and 1 – 4 for mode width, which provides over 157,000 possible sea spray mode solutions (Table 3). The range of fitting parameters were chosen to reflect those reported in laboratory experiments and field measurements (Table 6; Prather et al., 2013; Modini et al., 2010; Modini et al., 2015; Quinn et al., 2017; Saliba et al., 2019). Similar look-up tables have previously been used for optical measurement inversions (e.g., Lv et al., 2018; Veselovskii et al., 2002).

Deleted: Table 3

The scattering coefficients ($b_{sca,MIE}(\lambda)$) are then related to the size distribution by integrating Eq. (2) over all particle diameters (0.01 – 10 µm),

$$b_{sca,MIE}(\lambda) = \int_0^{\infty} \frac{\pi D_p^2}{4} Q_{sca}(\lambda, m, D_p) \frac{dN}{dlogD_p} dlogD_p \quad (2).$$

Q_{sca} is the scattering efficiency, λ is the light wavelength, and m is the particle core refractive index ($m = n + ik$). To match the NEPH and UHSAS RH of 55% during LASIC (Section 2.1.2), a constant m value of 1.45 + i0 was selected to simulate sea spray particle scattering. This value is lower than the average refractive index reported for dry sea salt (real component = 1.5 – 1.6, imaginary component < 10^{-6}) (Wang and Rood, 2008; Randles et al., 2004; Bi et al., 2018) and was calculated as a mass-weighted mixture of salt with water, where water has a refractive index of 1.33 (Wang and Rood, 2008) (SI Text 2). We found no substantial variation in the retrieved fit parameters for the range of 1.4 + 0i to 1.6 + 0i, but correlations to sea spray tracers (chloride and wind speed) were lower for 1.40 + i0 (high RH) and 1.6 + i0 (low RH) (SI Text 2). The mid-range value of m = 1.45 + i0 was used to approximate the scattering of sea salt for the measured RH of 55%.

Deleted: Within the Mie simulation, the refractive index, m, is assumed to be constant at 1.56 + 0i, which is typical for sea salt particles (Bi et al., 2018; Kent et al., 1983). This value provides a reasonable estimate of the scattering at marine sites where sea salts contribute a majority of supermicron scattering mass, with organic components contributing minor if not offsetting differences to the refractive index.

3.2 Selecting the Most Probable Mie Solutions

Deleted: High Probability Mie Solutions

Since many solutions are within the constraints of three wavelengths of measurements, we use the error between the nephelometer scattering and the Mie theory solutions to remove mode solutions that are not within the calculated error. The probability of solutions that meet the error threshold are then evaluated and only the top 5% most probable solutions are selected.

The measured supermicron scattering coefficient ($b_{sca,1-10\mu m}(\lambda)$) is compared to scattering coefficients computed for each simulated sea spray size distribution and Mie theory value of $b_{sca,MIE}(\lambda)$ in the look-up table by calculating the absolute error at each wavelength (λ), using Eq. (3):

$$\Delta b_{sca}(\lambda) = \left| b_{sca,1-10\mu m}(\lambda) - b_{sca,MIE}(\lambda) \right| \quad (3).$$

The scattering error ($\Delta b_{sca,RGB}$) is then computed by propagating the absolute error at each wavelength following Eq. (4):

$$\Delta b_{sca,RGB} = \sqrt{\sum_{\lambda=R,G,B} [\Delta b_{sca}(\lambda)]^2} \quad (4).$$

The total sample space is then reduced by selecting solutions from the look-up table that fall below the error threshold ($\sigma_{sca,RGB}$) calculated for that measurement time,

$$\Delta b_{sca,RGB} < \Delta \sigma_{sca,RGB} \quad (5a),$$

where,

$$\Delta \sigma_{sca,RGB} = \sqrt{\sum_{\lambda=R,G,B} \left[\left(\sigma_{sca,1-10\mu m}(\lambda) \right)^2 + \left(\sigma_{sca,inst} \right)^2 \right]} \quad (5b).$$

This error threshold incorporates the measured scattering variability at each wavelength for the averaging period ($\sigma_{sca,1\text{-}10\mu m}(\lambda)$) and accounts for the instrument error ($\sigma_{sca,inst}$, which is constant; Table 2). Figure 5 illustrates a time series of these error thresholds and the percent reduction of the Mie solution sample space (N = 157,850) for each retrieval during the background season of the LASIC. Using these error thresholds, the solution space is reduced by 98% on average with a range of 83 – 99% reduction, resulting in approximately 1000 – 2000 possible solutions each time.

The majority of solutions that are below the error threshold typically have a sea spray mode shape similar to those previously reported in literature (Quinn et al., 2017; Saliba et al., 2019; Bates et al., 2012), namely mass mean diameters within or near the coarse mode size range (1 – 10 µm) and mode width of 2 – 3, decreasing to below 0.1 cm^{-3} number concentration before the 10 µm cutoff. However, some of the solutions that meet the error threshold criterion are either too wide or large relative to the reported range of sea spray modes (Table 6, Fig. S4), which is a limitation of having only three scattering wavelengths to constrain the mode. To remove the outlier solutions and to reduce the sample space to a more consistent group of solutions, we apply a restriction on Mie solutions to consider only the most probable fitting parameters (N_T, D_g, σ_g) based on their frequency of occurrence. To demonstrate this restriction, we considered the normalized probabilities of the fitting parameters from Mie solutions that fall below the scattering error threshold, $\Delta \sigma_{sca,RGB}$, for one retrieval during LASIC (Fig. 6a-c). This retrieval was selected as its $\Delta \sigma_{sca,RGB}$ was within the average value for all LASIC observations during the clean marine background season (3.1 ± 2.1 Mm^{-1}) and is representative of most cases assessed.

Deleted: campaign

Deleted: is

Deleted: a few

Deleted: , but

Deleted: 5

Deleted: 2

Deleted: restrict

Mie solutions that meet the error threshold constrained the mode number concentration (N_T) and mean diameter (D_g) of the sea spray mode as shown by likely (probability > 75%) N_T and D_g falling within narrow ranges of the low error solutions (4% and 10% of the sample space, respectively) compared to a less constrained range for σ_g (45% of the sample space) (Fig. 6a-c). Since σ_g has a wider range of probable values, this parameter is effectively constrained by considering the joint probabilities of $N_T|\sigma_g$ and $D_g|\sigma_g$. These probabilities are computed as

$$P(N_T, \sigma_g) = P(N_T|\sigma_g) \cdot P(\sigma_g) \quad (6)$$

$$P(D_g, \sigma_g) = P(D_g|\sigma_g) \cdot P(\sigma_g) \quad (7).$$

The highest joint probability values restrict solutions to localized regions of the solution space (Fig. 6d-e). Selecting only the upper 5th normalized probability percentile of joint probabilities further restricts the full Mie solution sample space by an additional 16% and 13% for $N_T|\sigma_g$ and $D_g|\sigma_g$, respectively (Fig. 6d,e).

To assess which of these joint probability restrictions provided the most realistic sea spray mode results, retrieved mass concentrations and fitting parameters during the clean marine background season of LASIC were compared (Fig. S5). Restricting low error solutions using $D_g|\sigma_g$ joint probability led to retrieved sea spray mass concentrations that were 20 – 30% higher than the $N_T|\sigma_g$ combination, had mean mass diameters smaller than $N_T|\sigma_g$ (0.68 ± 0.08 µm vs. 1.47 ± 0.17 µm), and much broader mode widths (3.8 ± 0.2 vs. 2.4 ± 0.3). Although the retrieved mass mean diameters using the $D_g|\sigma_g$ joint probability were within the range of reported values from literature (Table 6; Quinn et al., 2017; Saliba et al., 2019; Bates et al., 2012), the exceptionally broad widths outside of the reported range suggests that the restriction using $D_g|\sigma_g$ does not effectively constrain the mode width as well as the $N_T|\sigma_g$ combination. For these reasons, only sea spray modes with fitting parameters in the top 5th percentile of $N_T|\sigma_g$ joint probability are used for this method, resulting in typically 300 – 500 for each measurement time.

3.3 Perturbing the Size Distribution

Uncertainty and variability have been shown to impact the assumed size distributions and optical properties of aerosol using inversion techniques (Viskari et al., 2012; Frie and Bahreini, 2021). Here, instrument uncertainty and measurement variability are incorporated into the fitting method by introducing random noise into the size distribution based on the size (σ_D) and number concentration ($\sigma_{PNSD,meas}(D_p)$, $\sigma_{PNSD,inst}$) uncertainties (Section 2.1.3; Table 2). Perturbations are simultaneously made to the measured number size distribution and particle diameters. Each bin of the size distribution is perturbed by introducing Gaussian noise that samples a random number from a normal distribution. The sampled normal distribution is defined by mean

Deleted: In order to account for the variability from averaging the measured size distribution over some time period when fitting the Mie solutions to the size distribution

Deleted: ,

Deleted: is introduced

Deleted: This

Deleted: method uses the MATLAB function *normrn* (The Mathworks Inc., version R2019b) to

Deleted: e

Deleted: into each bin of the size distribution by generating

Deleted: sampled

(μ) and standard deviation (σ) parameters where μ is the measured PNSD averaged over the time interval ($\sigma_{PNSD,meas}(D_p)$) and σ is the combined errors of the temporal variability and instrument concentration uncertainty (which is constant),

$$\sigma = \sqrt{\left(\sigma_{PNSD}\left(D_p\right)\right)^2 + \left(\sigma_{PNSD\ inst.}\right)^2} \quad (6).$$

The diameters in the size distributions are perturbed by shifting the size bins by the same value with a μ of 0 and σ as the instrument size uncertainty (σ_D). Size distributions are perturbed 100 times to provide a sample space of $N_{perturb}$ + 1 (the measured size distribution and 100 perturbations). Each probable Mie solution retrieved in Section 3.2 is then tested for the $N_{perturb}$ + 1 cases within the fitting region of the measured submicron size distribution described in Section 3.4.

Deleted: using *normrnd*

3.4 Fitting Modes to the Measured Size Distribution

The last step in retrieving sea spray modal properties is to select Mie solutions that most closely match the shape of the measured size distribution in a specified fitting region. Given the correlation of supermicron scattering and sea spray mass concentration during clean marine conditions (Chamaillard et al., 2006; Kleefeld et al., 2002; Quinn et al., 1998), all PNSDs are converted to particle mass size distributions (PMSDs) using

Deleted: Considering the correlated relationship between

$$\frac{dM}{dlogD_p} = \frac{\pi}{6}\,\rho\,D_p^3\,\frac{dN}{dlogD_p} \quad (7),$$

with the assumptions of spherical particle homogeneity and constant sea spray density, ρ. UHSAS and NEPH measurements were collected at 55% RH, so 1.3 g cm^{-3} was used as the estimated sea spray particle density by calculating a mass-weighted mixture of salt with water (SI Text 3).

To account for the consistent UHSAS artifacts at 0.6 and 0.85 μm (Section 2.1.1), we restricted the measured size distributions used to fit the Mie theory-simulated size distributions for diameters larger than 0.4 μm (0.4 to 1 μm UHSAS range) to 0.38 – 0.83 μm (the closest UHSAS diameter size bins within the specified range), which weights the comparison toward smaller sizes and effectively reduces the influence of the largest artifact while maintaining the shape of the accumulation mode "shoulder" (Fig. 1). For each Mie solution ($PMSD_{MIE}$), a residual sum of squares is computed between the measured and perturbed PMSDs as,

$$Fit\ RSS_{(j,k)} = \sum[PMSD_{(D,j)} - PMSD_{MIE(D,k)}]^2 \quad (8),$$

where index *j* represents each measured or perturbed size distribution and *k* is the index of the low error Mie solution. The fit RSS provides a quantifiable metric for comparing the scattering-retrieved mode to the expected sea spray fitting region. Chi-square "goodness of fit" calculations were also calculated and provided similar retrieved sea spray modal properties to those retrieved using the fit RSS minimization. The high probability Mie solution with minimum fit RSS for the measured and noise-perturbed size distributions is chosen to establish a range of mode fits. This Monte Carlo approach allowed for the selection of Mie solutions that capture the shape of the accumulation mode "shoulder" given uncertainties associated with measurement variability and instrument error and provides a statistically robust sample space for retrieving a unique sea spray mode solution. From the range of fit RSS-minimized sea spray modes, 95% confidence intervals of each fitting parameter are calculated to further constrain the most probable solution that fits the measured size distribution in the expected sea spray size range. On average, 30 – 40 solutions remain from this perturbation analysis for each measurement time with variabilities of 4% in number concentration, 3% in geometric mean diameter, and 1% in geometric standard deviation based on the sample means and upper and lower limits of the 95% confidence intervals. The low variabilities of these fitting parameters demonstrate consistent mode retrievals within the perturbations and stability of the retrieval procedure. Lastly, the fitting parameter solutions that are both highly probable (Section 3.2) and within the 95% confidence interval of fit RSS-minimized modes are averaged to produce a single lognormal sea spray mode with uncertainty of the solution defined as the upper and lower bounds of the 95% confidence interval.

Deleted: low error-restricted

Deleted: size distribution

4 Evaluation of NEPH-constrained Sea Spray Retrieval using Supermicron Size Measurements

This UHSAS-NEPH method was developed for LASIC measurements because that study lacked supermicron size distribution measurements. To evaluate the performance of this nephelometer-constrained sea spray mode retrieval, we first compared the scattering-constrained retrieval method during clean marine periods of the first cruise of the North Atlantic Aerosols and Marine Ecosystems Study (NAAMES 1) deployed 6 November – 30 November 2015 (Behrenfeld et al., 2019; Saliba et al., 2019), for which sea spray mode retrievals using supermicron size distributions and salt mass concentrations were also available. NAAMES 1 was selected as a case study of the nephelometer constraint on supermicron size because it had the most persistent clean conditions of the four ship deployments (Saliba et al., 2020). The low particle concentrations during NAAMES 1 (median CN_{total} = 94 cm^{-3}) also included the lowest sea spray aerosol concentrations (mean $N_{sea\ spray}$ = 5 cm^{-3}) of the four cruises (Saliba et al., 2019).

During NAAMES 1, submicron (0.1 – 0.8 µm) and supermicron (0.5 – 10 µm) size distributions were measured by a Scanning Electrical Mobility Spectrometer (SEMS, model 2002 BMI) and an Aerodynamic Particle Sizer (APS; model 3321 TSI), respectively. Scattering coefficients at < 1 µm and < 10 µm diameter size cuts were measured by a 3-λ (450, 550, 700 nm) integrating nephelometer (model 3563, TSI). In contrast to the LASIC measurements, nephelometer and size distribution measurements were operated at dry conditions (RH < 40%), meaning that dry particle properties could be assumed. Offline analysis of filters using ion chromatography provided size-resolved <10 µm salt (Na^+) mass concentrations at a 24-h resolution.

Saliba et al. (2019) retrieved the sea spray aerosol mode by fitting a lognormal mode to the shoulder of the merged ambient size distributions (SEMS-APS) during NAAMES 1. This method expanded upon the techniques described in previous work for fitting lognormal modes to measured marine size distributions (Modini et al., 2015; Quinn et al., 2017; Hussein et al., 2005) by allowing for the diameter and width of the mode to vary without laboratory constraints, which, when constrained, frequently retrieved parameters close to the interval limits. 15-min averaged < 10 µm SEMS-APS sea spray mode mass concentrations during NAAMES 1 were previously compared to the filter measurements of < 10 µm Na^+ mass and wind speed and found correlations of 0.7 and 0.6, respectively (Saliba et al., 2019). These correlations support the interpretation of the SEMS-APS retrieved mode as sea spray aerosol. For comparison of the UHSAS-NEPH retrieval method during 2-h NAAMES 1 measurements, SEMS was used as a replacement for UHSAS (SEMS-NEPH) with refractive index (m = 1.56 + 0i) and sea spray particle density (2.0 g cm^{-3}) for dry conditions.

Figure 7 and Table 4 show comparisons of the SEMS-APS and SEMS-NEPH sea spray retrievals for 2-h averaged SEMS, APS, and nephelometer measurements. SEMS-NEPH estimates the sea spray mode with double the number concentration, but only 10% more mass concentration on average than SEMS-APS (Fig. 7a,d). The main differences between these two variables can be explained by the retrieval constraints of each method: SEMS-APS constrains the number size distribution while the Mie-based scattering constraint of SEMS-NEPH is dependent upon the mass concentration. The difference in retrieved number concentrations between the two methods may have implications for attributing particle contributions to CCN. A factor of 2 difference between SEMS-NEPH and SEMS-APS estimates of particle number could modify the commonly observed 10 – 30% contribution of sea spray to CCN at supersaturations of 0.1 – 0.4% (Quinn et al., 2017; Sanchez et al., 2021; Modini et al., 2015) as more particles contribute to an already low CCN concentration during clean marine conditions.

The majority of integrated mass comparisons fall within a reasonable range of the 1:1 line except for some periods of low SEMS-APS mass concentrations (< 3 µg m^{-3}) (Figure 7d). The larger mass concentration estimates of SEMS-NEPH could be attributable to observed supermicron sea spray mass from the nephelometer that is not fully resolved by the APS number concentration estimate. This is supported by a stronger correlation of retrieved mass with supermicron scattering for SEMS-NEPH (R = 0.72) than what is observed using SEM-APS (R = 0.56) (Fig 7f), although it should be noted that the supermicron scattering has been used to constrain SEMS-NEPH solutions. Since the width of the sea spray mode from the scattering-based retrieval has been shown to be a poorly constrained parameter and is often narrower for SEMS-NEPH (2.0 ± 0.3) than SEMS-APS (2.4 ± 0.3), it may be the source of discrepancies between the other modal properties (Fig. 7c). These discrepancies are particularly apparent for the mode diameters, which are 20% larger in mean number size and 30% smaller in mean mass size for SEMS-NEPH in comparison to SEMS-APS. The scattering-based approach uses the probability occurrence of modal width to retrieve an optimal value, but the lack of number size distribution measurements at larger sizes (> 0.8 µm) from the SEMS provides insufficient information to constrain this parameter.

For the 2-h averaged concentrations, sea spray mass concentrations show moderate correlations of 0.50 for SEMS-APS and 0.53 for SEMS-NEPH with wind speed (Fig. 7g). The SEMS-APS correlation of mass to wind speed is slightly weaker than the correlation previously reported by Saliba et al. (2019) for 15-min averages (R = 0.6), but maintains a moderate correlation suggesting that the estimated mass concentration from both retrievals can be attributed to sea spray production by wind. Ambient < 10 µm sodium (Na^+) mass analyzed with ion chromatography moderately correlates with the SEMS-NEPH retrieval of sea spray mass (Fig. 7h). Although the SEMS-NEPH correlation is weaker than the mass concentration correlation to sodium using SEMS-APS (R = 0.7), the SEMS-NEPH correlation is consistent with other studies merging measured sub- and super-micron size distributions to fit sea spray modes and estimate salt mass in clean marine conditions (Quinn et al., 2017; Modini et al., 2015). Together these results show the efficacy of nephelometer-constrained estimates of supermicron sea spray particles. The moderate correlations and relative agreement between parameters of the retrieval methodologies with sea spray tracers indicate reasonable retrievals at dry relative humidity, even though supermicron size distributions provide more accurate retrieval of sea spray number properties.

5 Performance of UHSAS-NEPH Retrievals

For LASIC, sea spray modal properties were retrieved for 906 of the 909 2-h clean marine background periods using UHSAS-NEPH. The 3 periods for which the sea spray mode could not be retrieved were due to missing supermicron scattering measurements for at least one wavelength. To ensure that the algorithm retrievals were sufficiently consistent with both UHSAS and NEPH and representative of marine aerosol, we restricted the results to those with (1) low residual errors between the retrieval and measurements in the fitting region (0.38 – 0.83 µm), (2) low measured scattering variability during each 2-h time period, and (3) limited influence from potential non-marine aerosol sources, namely CN_3 concentrations < 400 cm^{-3}.

The fit RSS (Section 3.4) is the difference between the measured size distribution fitting region and the Mie solution determined from 3-wavelength supermicron scattering. Low residuals (fit RSS < 2) indicate good agreement between the measured region of the accumulation mode "shoulder" (0.38-0.83 µm) and the modal fit retrieved from scattering, hence low RSS shows the retrieved mode is well constrained by the measured UHSAS size distribution and NEPH scattering. The average fit RSS for the LASIC dataset that met the marine criteria was 1.26 ± 0.89 (Fig. 8a), which indicates that the retrieved modes are generally within the uncertainty of the measured size distribution in the 0.38 – 0.83 µm fitting region, but solutions that are not constrained by the UHSAS size distribution are also retrieved as evident by large values of fit RSS for various retrieval periods (Fig. 8a). A visual inspection of the retrieved mode fits suggested that values exceeding a residual threshold of 5 should be rejected as there is not sufficient agreement in the overlap region to consider the solution acceptable. Retrieved modes with fits above this threshold tended to have solutions that were either larger than the measured accumulation mode "shoulder" or had peaks in regions that the size distribution was low. These high fit RSS likely indicate that the supermicron scattering measurements were influenced by particles other than sea spray, which were not effectively constrained by the supermicron

Deleted: 4
Deleted: 1237
Deleted: 1240
Deleted: the
Deleted: algorithm to simultaneously fit size distributions
Deleted: ,
Deleted: were restricted
Deleted: (3) dry or near-dry nephelometer relative humidity (< 60%), and
Deleted: 4
Deleted: 9
Deleted: 2.4
Deleted: 1.4
Deleted: 6
Deleted: s

scattering. We also examined RSS thresholds of 1 through 10. There were no significant changes in correlations to wind speed or chemical signatures (Section 5.2) for lowering the threshold to values of 1 – 4, and there were decreases in those correlations for thresholds above a value of 6 (SI Table 7).

To assess the limitations of the algorithm due to the observed variability in measured scattering, we examined the relationship between the scattering error threshold and the fit RSS. The scattering error threshold, $\Delta\sigma_{sca,RGB}$, is defined as the combined effect of temporal variability and instrument uncertainty and had an average value of 3.1 ± 2.1 Mm^{-1} during LASIC. Low fit RSS (< 5) appear to coincide with low values of $\Delta\sigma_{sca,RGB}$ (R= 0.39), which suggests well-constrained sea spray mode solutions when the nephelometer scattering variability was low during the 2-h average (Fig. 8b). The relationship of low $\Delta\sigma_{sca,RGB}$ with low fit RSS generally persists to a threshold value of about $\Delta\sigma_{sca,RGB}$ = 5 Mm^{-1} before the fit RSS values increase in magnitude. Using this observed relationship between $\Delta\sigma_{sca,RGB}$ and fit RSS as a measure of the algorithm being sufficiently constrained to provide reasonable fits, we applied a restriction of acceptable scattering uncertainty tolerance of 5 Mm^{-1}.

Figure 8c illustrates a moderate correlation between fit RSS and CN_3 concentration (R = 0.58). Fit RSS is generally below the threshold of 5 for CN_3 concentrations less than 400 cm^{-3}. Above this concentration the fit RSS increases to higher values more consistently. The 600 cm^{-3} CN_3 criterion used to screen for clean periods is above the average and variability of the clean marine background season after the restriction was applied (300 ± 90 cm^{-3}). Because supermicron sea spray particles contribute low number concentrations to the aerosol budget, increases in particle number concentration likely indicate non-marine aerosol sources that were not excluded by the < 600 cm^{-3} clean marine criteria applied here. Therefore we have excluded periods when the total aerosol concentrations exceeds 400 cm^{-3} from the retrieval evaluation.

This additional screening of the LASIC dataset after applying the restriction of fit RSS (< 5), scattering error tolerance (< 5 Mm^{-1}), and using CN_3 < 400 cm^{-3} provided sea spray mode retrievals for 88% (794) of the available clean marine background periods during LASIC. These 794 sea spray retrievals were used to evaluate UHSAS-NEPH during LASIC.

6 Evaluation of UHSAS-NEPH Sea Spray Retrieval during LASIC

Since sea salt composition measurements were not collected during the LASIC campaign, four methods were used to evaluate sea salt identification: (1) comparison of UHSAS-NEPH to a modified version of a sea spray size distribution fitting algorithm that has been validated previously with salt composition (Saliba et al., 2019; Modini et al., 2015; Quinn et al., 2017), (2) correlation to the non-refractory chloride signal measured by the aerosol chemical speciation monitor (ACSM), (3) correlation of supermicron scattering and sea spray mass, where coarse scattering is taken as a tracer for sea spray during clean marine conditions (Kleefeld et al., 2002; Chamaillard et al., 2006; Quinn et al., 1998), and (4) correlation of retrieved mass to wind

Deleted: were

Deleted:

Deleted: 6

Deleted: 6

Deleted: d

Deleted: on average

Deleted: (

Deleted:)

Deleted: 5

speed, since it is widely used as a proxy for sea spray mass production (Lewis and Schwartz, 2004) and model flux parameterization (Gong, 2003; De Leeuw et al., 2011; Ma et al., 2008).

6.1 UHSAS-only Comparison

We applied the SEMS-APS fitting algorithm described in Section 4 to measured UHSAS number size distributions (hereafter identified as UHSAS-only) and compared sea spray mode results with those retrieved using UHSAS-NEPH. Sanchez et al. (2021) have recently applied the algorithm to submicron UHSAS size distributions obtained from aircraft measurements in the marine boundary layer of the Southern Ocean and found it to be a good approximation of sea spray contribution to CCN number concentration by comparison to quantified sub- and supermicron sea salt particles using electron microscopy. The mode fitting parameters N_T and D_g of the UHSAS-only method were converted to mass-derived values for comparison with UHSAS-NEPH using Eq. (7) for the same particle diameter range (D_p = 0.01 – 10 µm). UHSAS-only sea spray modes were fit for 90% of the 2-h average size distributions during the clean marine background season. Times that could not be fit generally included noise in the measured size distribution or other common singularities (see supplement of Saliba et al. (2019). Summary statistics comparing parameters retrieved using UHSAS-NEPH and UHSAS-only are provided in Table 5.

Integrated sea spray mode mass concentrations ranged from 0.008 to 23.5 µg m^{-3} employing UHSAS-only and 0.18 to 23.0 µg m^{-3} with UHSAS-NEPH. Average sea spray mass concentrations of 1.3 ± 2.2 µg m^{-3} and 8.37 ± 4.1 µg m^{-3} were observed for UHSAS-only and UHSAS-NEPH, respectively, which indicates that using UHSAS-only provides lower sea spray mass retrievals because UHSAS-only fits are constrained solely by the accumulation mode shoulder. Sea spray mass concentrations from both methods exhibit generally consistent concentrations during the clean marine periods of LASIC with no apparent seasonality (Fig. 9a), but there are distinct differences in the retrieved mode diameters and widths (Fig. 9b,c).

Sea spray mode retrievals using UHSAS-only were much smaller in mean mass diameter than UHSAS-NEPH with averages of 0.68 ± 0.01 µm and 1.47 ± 0.17 µm respectively (Fig. 9b). The range of mass mean diameters were similar for both retrieval methods, 0.4 to 1.6 µm for UHSAS-only and 0.6 to 1.9 µm for UHSAS-NEPH, though the majority of UHSAS-only mean diameters were submicron (Fig. 9b). Just over 2% (14) of UHSAS-only retrievals had mass mean diameters in the coarse mode (> 1 µm) compared to 91% (723) of UHSAS-NEPH. The peak in mass mean diameters at sizes within the coarse mode using UHSAS-NEPH can be attributed to the additional contributions of supermicron mass identified by the nephelometer supermicron scattering that are not constrained by the UHSAS submicron size distribution. These predominately supermicron mean diameters are consistent with the assumption of sea salt particles contributing a large amount of mass and scattering within the coarse mode, which is simply not captured by the submicron UHSAS distributions alone.

On average, UHSAS-only retrievals were narrower at 1.8 ± 0.4 than those retrieved with UHSAS-NEPH at 2.4 ± 0.3 (Fig. 9c). The range of mode widths using UHSAS-only varied from particularly narrow (1.3) to a fairly broad and unconstrained

Deleted: above

Deleted: (Saliba et al., 2019) optimized this procedure for merged number size distributions from a differential mobility analyzer and aerodynamic particle sizer covering a dry particle size range of 0.02 – 10 µm in the remote North Atlantic.

Deleted: 4

Deleted: 42

Deleted: 0.13 to 20.7

Deleted: 6.6 ± 3.5

Deleted: 7

Deleted: 7

Deleted: 1.3 ± 0.15

Deleted: 7

Deleted: 1.6

Deleted: 92

Deleted: 847

Deleted: 2

Deleted: 2

Deleted: 7

width of 5.3, compared to 1.1 to 3.97 for UHSAS-NEPH. UHSAS-only widths are determined solely by the shape of the large accumulation mode shoulder in the UHSAS number size distribution and include a variety of widths based on how flat or sharp the slope of this shoulder may be. Mode widths retrieved from both methods were predominately narrower than a value of 3 with only 2% of UHSAS-only modes and 1% of UHSAS-NEPH modes greater than this value. Average UHSAS-only mode narrowness again reflects the absence of supermicron size distribution measurements. Sanchez et al. (2021) reported a similarly narrow average mode width (1.44 ± 0.25) for marine boundary layer sea spray aerosol retrieved with UHSAS-only. Conversely, Yu et al. (2019) reported a broad mode width (geometric standard deviation of 2.7) and volume peak at supermicron diameter (approximately 2 µm) for 24-h averaged sea salt particle size distributions at Ascension Island using Aerosol Robotic Network retrievals, which is more consistent with UHSAS-NEPH observations. These results indicate that UHSAS-only may provide a good estimate of sea spray number concentration, which predominantly consists of submicron-sized particles (Sanchez et al., 2021), but the lack of supermicron measurements makes it unable to adequately identify mass contributions from larger particles.

Comparing the sea spray mode fitting parameters to those found in literature shows that retrieved modal properties for both methods are within the range of reported values of mass mean dry diameter (0.25 – 1.6 µm) and mode width (1.4 – 3) (Fig. 9b,c and Table 6), while noting that these LASIC retrievals are for 55% RH. The median of reported mass diameter (0.88 µm) falls in between the statistical mode values (peaks in histograms) of the retrieval methods at the upper end of UHSAS-only and lower end of UHSAS-NEPH (Fig. 9b), showing consistency with other ambient sea spray mode measurements (Quinn et al., 2017; Sanchez et al., 2021; Modini et al., 2015). Retrievals using only the UHSAS number size distributions generally show better agreement in terms of mode size with laboratory-based bubble bursting and breaking wave flume studies, which had mass mean diameters that were less than 1 µm (Prather et al., 2013; Bates et al., 2012; Modini et al., 2010). UHSAS-NEPH retrievals are more consistent with field observations of the sea spray size distribution across several ocean basins, including open ocean studies in the Pacific and Atlantic, in which measurements of supermicron size distributions were incorporated (Quinn et al., 2017; Saliba et al., 2019; Modini et al., 2015). The UHSAS-NEPH retrieval of sea spray mode width was on the lower end of the reported laboratory and field measurement values, while the narrow UHSAS-only modes were generally outside the spread of the majority of reported values. These differences of the ranges in retrieved values show that the mode width is the least constrained parameter derived by UHSAS-only and UHSAS-NEPH, although the scattering-based constraint provides some apparent improvement compared to UHSAS-only when supermicron mass contributions are considered.

Figure 10 displays six UHSAS-NEPH sea spray mode fits that are characteristic of the retrieval procedure. Cases of different modal properties (diameter, width, mass) and the comparison of this retrieval with the UHSAS-only algorithm are presented. For both methods, the accumulation mode (0.4 – 1 µm) is generally well characterized by the retrieved modes following the shape of this broad shoulder closely. Differences between the UHSAS-only and UHSAS-NEPH retrieved mass size

Deleted: 2

Deleted: 7

Deleted: 7

Deleted: 5

Deleted: mode

Deleted: 7

Deleted: 8

Deleted: applied to clean marine background observations during LASIC…

distributions become more apparent just before the 1 µm size limit of the UHSAS. For narrow modes (σ_g ~ 2), using the UHSAS-only method appears to generally be sufficient for quantifying sea spray mode mass concentration in the absence of supermicron scattering measurements (Fig. 10a). In these cases, the lower contribution of coarse particles measured by the nephelometer supermicron scattering adds little information at the tail of the size distribution. The limitations of fitting a sea spray mode based solely on the shape of the accumulation mode "shoulder" in the number size distribution are illustrated in Fig. 10b,c,d. The broadness of the shoulder at submicron sizes (0.38 – 0.83 µm) forces the UHSAS-only retrieval to include more particles from submicron sizes and fewer from the supermicron regime. This leads to lower mass concentrations in UHSAS-only compared to UHSAS-NEPH. Mode retrievals using only the UHSAS size distribution likely underestimate much of the mass at supermicron sizes as seen in the UHSAS-only modes tailing off more sharply in the coarse regime (Fig. 10b,c,e,f), with up to 5 µg m^{-3} of sea spray mass difference in the cases considered here.

6.2 Sea Spray Tracers

We next compared sea spray mode mass concentrations from UHSAS-only and UHSAS-NEPH with available sea spray tracers to evaluate the extent to which the retrieved modal properties represent realistic sea spray size distributions.

The submicron mass concentration measured by the ACSM provided a trace chloride signal that could be used to examine sea salt mass concentrations from the UHSAS-only and UHSAS-NEPH retrievals. Comparing retrieved submicron sea spray mass with the ACSM chloride mass, we found correlations of R = 0.39 ($p < 0.05$) for UHSAS-only and R = 0.35 ($p < 0.05$) for UHSAS-NEPH (Fig. 11a,b). While the ACSM signal is a very indirect chemical measurement of refractory chloride, these positive correlations provide support for the ability of both methods to identify retrieved modes as sea spray. The higher correlation of UHSAS-only over UHSAS-NEPH may be a result of the submicron sampling range of the ACSM, the diameter range in which UHSAS-only is solely constrained. Additionally, much of the sea spray mass retrieved from UHSAS-NEPH is concentrated in the supermicron regime, which is not observed in ACSM submicron chloride measurements.

Correlations between sea spray mass and the supermicron scattering coefficient were assessed for UHSAS-only and UHSAS-NEPH using retrievals that followed the criteria discussed in previous sections. Sea spray mass concentrations from UHSAS-only were consistently less than 2 µg m^{-3} and were not able to quantitatively explain the variability in the measured supermicron scattering at 550 nm, indicated by a very weak correlation (R^2 = 0.01, $p < 0.05$; Fig. 11c). Although the stronger correlation between sea spray mass concentration and scattering with UHSAS-NEPH (R^2 = 0.84, $p < 0.05$, Fig. 11d) is an expected result given that the retrieved modes are constrained by scattering measurements, the lack of correlation from UHSAS-only emphasizes the importance of including supermicron particle size measurements to adequately characterize how optical properties are influenced by the sea spray size distribution.

Deleted: <
Deleted: 8
Deleted: ,b
Deleted: 8
Deleted: ,f
Deleted: 8
Deleted: 5
Deleted: 43
Deleted: 2
Deleted: 9
Deleted: additional
Deleted: very
Deleted: coefficient of determination
Deleted: 2
Deleted: 0.02
Deleted: 9
Deleted: 2
Deleted: 0.72
Deleted: 9

The functional relationship between sea spray mass concentration and wind speed was evaluated using linear regression on UHSAS-only and UHSAS-NEPH retrievals and resulted in correlation coefficients of 0.1 and 0.2, respectively ($p < 0.05$) (Fig. 11e,f). These correlations were lower than values in the range of 0.4 to 0.9 reported for numerous basins of the global ocean (Liu et al., 2021; Russell et al., 2010; Feng et al., 2017; Saliba et al., 2019). The calm and generally invariant wind speed observed during the LASIC background season (7.1 ± 1.4 m/s) could explain the poor correlations for both methods as the lack of dynamic range in wind speed at Ascension Island reduces the degree to which it explains the variability in concentration. The variability may instead be impacted by marine airmass transport of sea spray aerosol from source regions away from Ascension that reach the island rather than local wind conditions, which would not be resolved in the correlation (Grythe et al., 2014). The improved correlation of UHSAS-NEPH in comparison to UHSAS-only shows some added value of applying the supermicron scattering constraint to characterize the sea spray mode. Evaluation of the method using North Atlantic measurements (Section 4), where more dynamic wind conditions were observed, shows that use of the supermicron scattering constraint could be comparable to the constraint of measured supermicron size distributions when estimating sea spray production from wind speed as has been done in previous work (Saliba et al., 2019; Modini et al., 2015; Quinn et al., 2017). These results indicate that the incorporation of nephelometer scattering as a constraint for supermicron particle size provides a reasonable replacement for measured supermicron mass size distributions.

7 Concluding Remarks

In this work we have presented a new method that combines measured submicron size distributions and 3-wavelength supermicron scattering to estimate observationally-constrained sea spray modal properties at a remote marine site using a Mie inversion (UHSAS-NEPH). When the retrieval was limited to marine periods with low aerosol concentration ($CN_3 < 400$ cm^{-3}), reasonable sea spray size distributions were obtained 88% of the time. UHSAS-NEPH had larger fit residuals for higher ambient scattering variability ($\Delta\sigma_{sca,RGB} > 5$ Mm^{-1}) and high relative humidity within the nephelometer (> 60%), which affected the consistency with which the Mie solutions could be constrained by scattering measurements and UHSAS submicron mass size distributions.

Retrieved sea spray modes ranged in mean mass diameter from 0.6 to 1.9 µm (1.47 ± 0.17 µm), modal width from 1.1 to 3.9 (2.4 ± 0.3), and mass concentration from 0.18 to 23.0 µg m^{-3} (8.37 ± 4.1 µg m^{-3}), which are consistent with other field-based measurements of the sea spray aerosol mode. By comparing retrieved modes to available tracers of sea salt, we have shown that estimates of supermicron size, such as from Mie Inversion techniques, are necessary to resolve expected sea spray mass correlations with scattering and wind speed at Ascension Island. The observed positive correlation of UHSAS-NEPH submicron sea spray mode mass with measured submicron chloride signal ($R = 0.35$) provided indirect chemical support of UHSAS-NEPH modes as sea spray. UHSAS-NEPH showed stronger correlations ($R = 0.84$) to the supermicron scattering in comparison to fitting only based on the submicron size distribution accumulation mode ($R = 0.01$), as expected from using the

Deleted: 9
Deleted: Extending this method to a case study in the
Deleted: are
Deleted: (Text S2, Fig. S6g)
Deleted: is
Deleted: ¶
Deleted: 6
Deleted: clean
Deleted: 95
Deleted: (dried)
Deleted: 6
Deleted: 3
Deleted: 2
Deleted: 2
Deleted: 7
Deleted: 2
Deleted: 2
Deleted: 3
Deleted: 0
Deleted: 7
Deleted: 6.5
Deleted: 3.5
Deleted: chloride,
Deleted: ,
Deleted: 2
Deleted: 2
Deleted: 72
Deleted: 2
Deleted: 2

scattering measurement to constrain UHSAS-NEPH solutions. Incorporation of scattering measurements as an estimate of supermicron mass concentration improved the weak wind speed correlation (R = 0.2) relative to using only the submicron size distribution (R = 0.1) for sea spray retrieval. This result was consistent with sea spray production even though the relationship was not as strong as that found in prior studies with a greater dynamic range of wind speed and available supermicron size distributions. Other environmental parameters such as sea surface temperature and its impacts on surface tension and kinematic viscosity could also be considered when assessing the relationship between sea spray production and modal properties relative to these retrieval methods at Ascension Island (Saliba et al., 2019; Liu et al., 2021; Salter et al., 2014), although salt measurements provided a more direct evaluation of the method when applied to North Atlantic observations (Section 4).

We have demonstrated that 3-wavelength scattering measurements constrained with submicron size distributions yield sea spray mode estimates that are consistent with sea salt during clean marine periods of LASIC. Inclusion of additional scattering wavelengths and chemical measurements of particles would provide additional constraints on refractive index and scattering efficiency by allowing for temporally resolved adjustments in parameters used for Mie simulations. The retrieval procedure outlined in this work is a self-contained code with look-up table and is available to the broader scientific community. Future use of this combined size distribution and scattering-based approach to other measured marine datasets that lack supermicron size distributions can expand the array of sea spray observations and improve upon size, mass, and emission characterization of marine aerosol in climate models, further constraining the uncertainty in natural aerosol impacts on radiative forcing.

Code Availability

The sea spray mode retrieval algorithm and Mie theory scattering look-up table are available as a MATLAB function and MATLAB matrix file at the UCSD digital archives (https://doi.org/10.6075/J0GT5NCR). The Mie codes used to simulate sea spray scattering are available at the same location.

Data Availability

All LASIC data are publicly available from the ARM data discovery (https://adc.arm.gov/discovery/) (last access: 5 January 2022). Specific direction to each measurement dataset are provided as DOI references in Table 1. Retrieved sea spray modal parameters using LASIC and NAAMES measurements can be found at the UCSD digital archives (https://doi.org/10.6075/J0GT5NCR). Scattering and chemical measurements from NAAMES 1 are available at https://saga.pmel.noaa.gov/data/download.php?cruise=NAAMES1 (last accessed: 18 April 2022); SEMS size distributions from NAAMES 1 are available at https://library.ucsd.edu/dc/object/bb0856963d (last accessed: 24 April 2022).

Deleted: NaCl

Deleted: chemical

Deleted: would

Deleted: evaluatio

Deleted: n

Author Contribution

Conceptualization and Methodology: **JLD, GS, LMR**. Code development, Formal Analysis**: JLD, GS, ASW**. Supervision and Funding acquisition: **LMR and DL**. Writing – original draft: **JLD**. **All authors** contributed to the review and editing of the manuscript.

Competing interests

The authors declare that they have no conflict of interest.

Financial Support

This research was supported by the Director, Office of Science, Office of Biological and Environmental Research, Climate and Environmental Sciences Division of the U.S. Department of Energy under Contract DE-SC0021045.

Acknowledgements

The authors graciously thank Paquita Zuidema, the LASIC science team, and ARM instrument mentors for their assistance in the interpretation of measured size distributions from SMPS and UHSAS, and nephelometer scattering measurements collected during the LASIC campaign. We thank Timothy Bates and Patricia Quinn for NAAMES 1 scattering and composition measurements. We also extend our thanks to Roya Bahreini for productive discussions on ways to incorporate measurement uncertainties and variabilities into the Mie Inversion methodology. The authors express thanks to Ian Eisenman for sharing computing resources that made the execution of Mie scattering simulations and sea spray retrieval possible. Two anonymous reviewers are thanked for their constructive comments that have helped improve the further development of the retrieval method and presentation of results in this study.

References

Anderson, T. and Ogren, J.: Determining aerosol radiative properties using the TSI 3563 integrating nephelometer, Aerosol Science and Technology, 29, 57-69, 10.1080/02786829808965551, 1998.

Anderson, T., Covert, D., Marshall, S., Laucks, M., Charlson, R., Waggoner, A., Ogren, J., Caldow, R., Holm, R., Quant, F., Sem, G., Wiedensohler, A., Ahlquist, N., and Bates, T.: Performance characteristics of a high-sensitivity, three-wavelength, total scatter/backscatter nephelometer, Journal of Atmospheric and Oceanic Technology, 13, 967-986, 10.1175/1520-0426(1996)013<0967:PCOAHS>2.0.CO;2, 1996.

Ayash, T., Gong, S., and Jia, C.: Direct and indirect shortwave radiative effects of sea salt aerosols, Journal of Climate, 21, 3207-3220, 10.1175/2007JCLI2063.1, 2008.

Bates, T., Quinn, P., Frossard, A., Russell, L., Hakala, J., Petaja, T., Kulmala, M., Covert, D., Cappa, C., Li, S., Hayden, K., Nuaaman, I., McLaren, R., Massoli, P., Canagaratna, M., Onasch, T., Sueper, D., Worsnop, D., and Keene, W.: Measurements of ocean derived aerosol off the coast of California, Journal of Geophysical Research-Atmospheres, 117, 10.1029/2012JD017588, 2012.

Behrenfeld, M., Moore, R., Hostetler, C., Graff, J., Gaube, P., Russell, L., Chen, G., Doney, S., Giovannoni, S., Liu, H., Proctor, C., Bolalios, L., Baetge, N., Davie-Martin, C., Westberry, T., Bates, T., Bell, T., Bidle, K., Boss, E., Brooks, S., Cairns, B., Carlson, C., Halsey, K., Harvey, E., Hu, C., Karp-Boss, L., Kleb, M., Menden-Deuer, S., Morison, F., Quinn, P., Scarino, A., Anderson, B., Chowdhary, J., Crosbie, E., Ferrare, R., Haire, J., Hu, Y., Janz, S., Redemann, J., Saltzman, E., Shook, M., Siegel, D., Wisthaler, A., Martine, M., and Ziemba, L.: The North Atlantic Aerosol and Marine Ecosystem Study (NAAMES): Science Motive and Mission Overview, Frontiers in Marine Science, 6, 10.3389/fmars.2019.00122, 2019.

Bi, L., Lin, W., Wang, Z., Tang, X., Zhang, X., and Yi, B.: Optical Modeling of Sea Salt Aerosols: The Effects of Nonsphericity and Inhomogeneity, Journal of Geophysical Research-Atmospheres, 123, 543-558, 10.1002/2017JD027869, 2018.

Bluvshtein, N., Lin, P., Flores, J., Segev, L., Mazar, Y., Tas, E., Snider, G., Weagle, C., Brown, S., Laskin, A., and Rudich, Y.: Broadband optical properties of biomass-burning aerosol and identification of brown carbon chromophores, Journal of Geophysical Research-Atmospheres, 122, 5441-5456, 10.1002/2016JD026230, 2017.

Bohren, C. F. and Huffman, D. R., KGaA, W. V. V. G. C. (Ed.): Absorption and Scattering of Light by Small Particles, John Wiley & Sons, Inc, 530 pp., 10.1002/9783527618156, 1998.

Brock, C., Williamson, C., Kupc, A., Froyd, K., Erdesz, F., Wagner, N., Richardson, M., Schwarz, J., Gao, R., Katich, J., Campuzano-Jost, P., Nault, B., Schroder, J., Jimenez, J., Weinzierl, B., Dollner, M., Bui, T., and Murphy, D.: Aerosol size distributions during the Atmospheric Tomography Mission (ATom): methods, uncertainties, and data products, Atmospheric Measurement Techniques, 12, 3081-3099, 10.5194/amt-12-3081-2019, 2019.

Bullard, R. L., Uin, J., Springston, S. R., Kuang, C., and Smith, S.: Aerosol Inlet Characterization Experiment Report, 2017.

Cai, Y., Montague, D., Mooiweer-Bryan, W., and Deshler, T.: Performance characteristics of the ultra high sensitivity aerosol spectrometer for particles between 55 and 800 nm: Laboratory and field studies, Journal of Aerosol Science, 39, 759-769, 10.1016/j.jaerosci.2008.04.007, 2008.

Chamaillard, K., Kleefeld, C., Jennings, S., Ceburnis, D., and O'Dowd, C.: Light scattering properties of sea-salt aerosol particles inferred from modeling studies and ground-based measurements, Journal of Quantitative Spectroscopy & Radiative Transfer, 101, 498-511, 10.1016/j.jqsrt.2006.02.062, 2006.

de Leeuw, G., Andreas, E., Anguelova, M., Fairall, C., Lewis, E., O'Dowd, C., Schulz, M., and Schwartz, S.: PRODUCTION FLUX OF SEA SPRAY AEROSOL, Reviews of Geophysics, 49, 10.1029/2010RG000349, 2011.

Delene, D. and Ogren, J.: Variability of aerosol optical properties at four North American surface monitoring sites, Journal of the Atmospheric Sciences, 59, 1135-1150, 10.1175/1520-0469(2002)059<1135:VOAOPA>2.0.CO;2, 2002.

DeMott, P., Hill, T., McCluskey, C., Prather, K., Collins, D., Sullivan, R., Ruppel, M., Mason, R., Irish, V., Lee, T., Hwang, C., Rhee, T., Snider, J., McMeeking, G., Dhaniyala, S., Lewis, E., Wentzell, J., Abbatt, J., Lee, C., Sultana, C., Ault, A., Axson,

J., Martinez, M., Venero, I., Santos-Figueroa, G., Stokes, M., Deane, G., Mayol-Bracero, O., Grassian, V., Bertram, T., Bertram, A., Moffett, B., and Franc, G.: Sea spray aerosol as a unique source of ice nucleating particles, Proceedings of the National Academy of Sciences of the United States of America, 113, 5797-5803, 10.1073/pnas.1514034112, 2016.

Denjean, C., Bourrianne, T., Burnet, F., Mallet, M., Maury, N., Colomb, A., Dominutti, P., Brito, J., Dupuy, R., Sellegri, K., Schwarzenboeck, A., Flamant, C., and Knippertz, P.: Overview of aerosol optical properties over southern West Africa from DACCIWA aircraft measurements, Atmospheric Chemistry and Physics, 20, 4735-4756, 10.5194/acp-20-4735-2020, 2020.

Denjean, C., Cassola, F., Mazzino, A., Triquet, S., Chevaillier, S., Grand, N., Bourrianne, T., Momboisse, G., Sellegri, K., Schwarzenbock, A., Freney, E., Mallet, M., and Formenti, P.: Size distribution and optical properties of mineral dust aerosols transported in the western Mediterranean, Atmospheric Chemistry and Physics, 16, 1081-1104, 10.5194/acp-16-1081-2016, 2016.

Di Biagio, C., Formenti, P., Balkanski, Y., Caponi, L., Cazaunau, M., Pangui, E., Journet, E., Nowak, S., Andreae, M., Kandler, K., Saeed, T., Piketh, S., Seibert, D., Williams, E., and Doussin, J.: Complex refractive indices and single-scattering albedo of global dust aerosols in the shortwave spectrum and relationship to size and iron content, Atmospheric Chemistry and Physics, 19, 15503-15531, 10.5194/acp-19-15503-2019, 2019.

Feng, L., Shen, H., Zhu, Y., Gao, H., and Yao, X.: Insight into Generation and Evolution of Sea-Salt Aerosols from Field Measurements in Diversified Marine and Coastal Atmospheres, Scientific Reports, 7, 10.1038/srep41260, 2017.

Frie, A. and Bahreini, R.: Refractive index confidence explorer (RICE): A tool for propagating uncertainties through complex refractive index retrievals from aerosol particles, Aerosol Science and Technology, 55, 703-717, 10.1080/02786826.2021.1895428, 2021.

Frossard, A., Russell, L., Burrows, S., Elliott, S., Bates, T., and Quinn, P.: Sources and composition of submicron organic mass in marine aerosol particles, Journal of Geophysical Research-Atmospheres, 119, 12977-13003, 10.1002/2014JD021913, 2014.

Fuentes, E., Coe, H., Green, D., de Leeuw, G., and McFiggans, G.: On the impacts of phytoplankton-derived organic matter on the properties of the primary marine aerosol - Part 1: Source fluxes, Atmospheric Chemistry and Physics, 10, 9295-9317, 10.5194/acp-10-9295-2010, 2010.

Gasso, S., Hegg, D., Covert, D., Collins, D., Noone, K., Ostrom, E., Schmid, B., Russell, P., Livingston, J., Durkee, P., and Jonsson, H.: Influence of humidity on the aerosol scattering coefficient and its effect on the upwelling radiance during ACE-2, Tellus Series B-Chemical and Physical Meteorology, 52, 546-567, 10.1034/j.1600-0889.2000.00055.x, 2000.

Gong, S.: A parameterization of sea-salt aerosol source function for sub- and super-micron particles, Global Biogeochemical Cycles, 17, 10.1029/2003GB002079, 2003.

Grythe, H., Strom, J., Krejci, R., Quinn, P., and Stohl, A.: A review of sea-spray aerosol source functions using a large global set of sea salt aerosol concentration measurements, Atmospheric Chemistry and Physics, 14, 1277-1297, 10.5194/acp-14-1277-2014, 2014.

Haywood, J., Francis, P., Osborne, S., Glew, M., Loeb, N., Highwood, E., Tanre, D., Myhre, G., Formenti, P., and Hirst, E.: Radiative properties and direct radiative effect of Saharan dust measured by the C-130 aircraft during SHADE: 1. Solar spectrum, Journal of Geophysical Research-Atmospheres, 108, 10.1029/2002JD002687, 2003.

Horowitz, H., Holmes, C., Wright, A., Sherwen, T., Wang, X., Evans, M., Huang, J., Jaegle, L., Chen, Q., Zhai, S., and Alexander, B.: Effects of Sea Salt Aerosol Emissions for Marine Cloud Brightening on Atmospheric Chemistry: Implications for Radiative Forcing, Geophysical Research Letters, 47, 10.1029/2019GL085838, 2020.

Howell, S., Freitag, S., Dobracki, A., Smirnow, N., and Sedlacek, A.: Undersizing of aged African biomass burning aerosol by an ultra-high-sensitivity aerosol spectrometer, Atmospheric Measurement Techniques, 14, 7381-7404, 10.5194/amt-14-7381-2021, 2021.

Humphries, R., Keywood, M., Gribben, S., McRobert, I., Ward, J., Selleck, P., Taylor, S., Harnwell, J., Flynn, C., Kulkarni, G., Mace, G., Protat, A., Alexander, S., and McFarquhar, G.: Southern Ocean latitudinal gradients of cloud condensation nuclei, Atmospheric Chemistry and Physics, 21, 12757-12782, 10.5194/acp-21-12757-2021, 2021.

Hussein, T., Dal Maso, M., Petaja, T., Koponen, I., Paatero, P., Aalto, P., Hameri, K., and Kulmala, M.: Evaluation of an automatic algorithm for fitting the particle number size distributions, Boreal Environment Research, 10, 337-355, 2005.

Kassianov, E., Berg, L., Pekour, M., Barnard, J., Chand, D., Flynn, C., Ovchinnikov, M., Sedlacek, A., Schmid, B., Shilling, J., Tomlinson, J., and Fast, J.: Airborne Aerosol in Situ Measurements during TCAP: A Closure Study of Total Scattering, Atmosphere, 6, 1069-1101, 10.3390/atmos6081069, 2015.

Keene, W., Maring, H., Maben, J., Kieber, D., Pszenny, A., Dahl, E., Izaguirre, M., Davis, A., Long, M., Zhou, X., Smoydzin, L., and Sander, R.: Chemical and physical characteristics of nascent aerosols produced by bursting bubbles at a model air-sea interface, Journal of Geophysical Research-Atmospheres, 112, 10.1029/2007JD008464, 2007.

Khlystov, A., Stanier, C., and Pandis, S.: An algorithm for combining electrical mobility and aerodynamic size distributions data when measuring ambient aerosol, Aerosol Science and Technology, 38, 229-238, 10.1080/02786820390229543, 2004.

Kishcha, P., da Silva, A., Starobinets, B., Long, C., Kalashnikova, O., and Alpert, P.: Saharan dust as a causal factor of hemispheric asymmetry in aerosols and cloud cover over the tropical Atlantic Ocean, International Journal of Remote Sensing, 36, 3423-3445, 10.1080/01431161.2015.1060646, 2015.

Kleefeld, C., O'Dowd, C., O'Reilly, S., Jennings, S., Aalto, P., Becker, E., Kunz, G., and de Leeuw, G.: Relative contribution of submicron and supermicron particles to aerosol light scattering in the marine boundary layer, Journal of Geophysical Research-Atmospheres, 107, 10.1029/2000JD000262, 2002.

Kupc, A., Williamson, C., Wagner, N., Richardson, M., and Brock, C.: Modification, calibration, and performance of the Ultra-High Sensitivity Aerosol Spectrometer for particle size distribution and volatility measurements during the Atmospheric Tomography Mission (ATom) airborne campaign, Atmospheric Measurement Techniques, 11, 369-383, 10.5194/amt-11-369-2018, 2018.

Lewis, E. R. and Schwartz, S. E., Union, A. G. (Ed.): Sea Salt Aerosol Production: Mechanisms, Methods, Measurements and Models, Geophysical Monograph Series, American Geophysical Union, 413 pp., 10.1029/GM152, 2004.

Liu, S., Liu, C., Froyd, K., Schill, G., Murphy, D., Bui, T., Dean-Day, J., Weinzierl, B., Dollner, M., Diskin, G., Chen, G., and Gao, R.: Sea spray aerosol concentration modulated by sea surface temperature, Proceedings of the National Academy of Sciences of the United States of America, 118, 10.1073/pnas.2020583118, 2021.

Lv, M., Wang, Z., Li, Z., Luo, T., Ferrare, R., Liu, D., Wu, D., Mao, J., Wan, B., Zhang, F., and Wang, Y.: Retrieval of Cloud Condensation Nuclei Number Concentration Profiles From Lidar Extinction and Backscatter Data, Journal of Geophysical Research-Atmospheres, 123, 6082-6098, 10.1029/2017JD028102, 2018.

Ma, X., von Salzen, K., and Li, J.: Modelling sea salt aerosol and its direct and indirect effects on climate, Atmospheric Chemistry and Physics, 8, 1311-1327, 10.5194/acp-8-1311-2008, 2008.

Mie, G.: Articles on the optical characteristics of turbid tubes, especially colloidal metal solutions., Annalen Der Physik, 25, 377-445, 10.1002/andp.19083300302, 1908.

Miller, M., Nitschke, K., Ackerman, T., Ferrell, W., Hickmon, N., Ivey, M., Turner, D., and Ellingson, R.: The ARM Mobile Facilities, Atmospheric Radiation Measurement (Arm) Program: the First 20 Years, 57, 10.1175/AMSMONOGRAPHS-D-15-0051.1, 2016.

Miller, R., McFarquhar, G., Rauber, R., O'Brien, J., Gupta, S., Segal-Rozenhaimer, M., Dobracki, A., Sedlacek, A., Burton, S., Howell, S., Freitag, S., and Dang, C.: Observations of supermicron-sized aerosols originating from biomass burning in southern Central Africa, Atmospheric Chemistry and Physics, 21, 14815-14831, 10.5194/acp-21-14815-2021, 2021.

Ming, Y. and Russell, L.: Predicted hygroscopic growth of sea salt aerosol, Journal of Geophysical Research-Atmospheres, 106, 28259-28274, 10.1029/2001JD000454, 2001.

Modini, R., Harris, B., and Ristovski, Z.: The organic fraction of bubble-generated, accumulation mode Sea Spray Aerosol (SSA), Atmospheric Chemistry and Physics, 10, 2867-2877, 10.5194/acp-10-2867-2010, 2010.

Modini, R., Frossard, A., Ahlm, L., Russell, L., Corrigan, C., Roberts, G., Hawkins, L., Schroder, J., Bertram, A., Zhao, R., Lee, A., Abbatt, J., Lin, J., Nenes, A., Wang, Z., Wonaschutz, A., Sorooshian, A., Noone, K., Jonsson, H., Seinfeld, J., Toom-Sauntry, D., Macdonald, A., and Leaitch, W.: Primary marine aerosol-cloud interactions off the coast of California, Journal of Geophysical Research-Atmospheres, 120, 4282-4303, 10.1002/2014JD022963, 2015.

Moore, R., Wiggins, E., Ahern, A., Zimmerman, S., Montgomery, L., Jost, P., Robinson, C., Ziemba, L., Winstead, E., Anderson, B., Brock, C., Brown, M., Chen, G., Crosbie, E., Guo, H., Jimenez, J., Jordan, C., Lyu, M., Nault, B., Rothfuss, N., Sanchez, K., Schueneman, M., Shingler, T., Shook, M., Thornhill, K., Wagner, N., and Wang, J.: Sizing response of the Ultra-High Sensitivity Aerosol Spectrometer (UHSAS) and Laser Aerosol Spectrometer (LAS) to changes in submicron aerosol composition and refractive index, Atmospheric Measurement Techniques, 14, 4517-4542, 10.5194/amt-14-4517-2021, 2021.

Mulcahy, J., O'Dowd, C., and Jennings, S.: Aerosol optical depth in clean marine and continental northeast Atlantic air, Journal of Geophysical Research-Atmospheres, 114, 10.1029/2009JD011992, 2009.

Murphy, D., Anderson, J., Quinn, P., McInnes, L., Brechtel, F., Kreidenweis, S., Middlebrook, A., Posfai, M., Thomson, D., and Buseck, P.: Influence of sea-salt on aerosol radiative properties in the Southern Ocean marine boundary layer, Nature, 392, 62-65, 10.1038/32138, 1998.

Mätzler, C.: Mie_abcd [code], 2002.

O'Dowd, C., Scannell, C., Mulcahy, J., and Jennings, S.: Wind Speed Influences on Marine Aerosol Optical Depth, Advances in Meteorology, 2010, 10.1155/2010/830846, 2010.

O'Dowd, C., Smith, M., Consterdine, I., and Lowe, J.: Marine aerosol, sea-salt, and the marine sulphur cycle: A short review, Atmospheric Environment, 31, 73-80, 10.1016/S1352-2310(96)00106-9, 1997.

Ovadnevaite, J., Ceburnis, D., Canagaratna, M., Berresheim, H., Bialek, J., Martucci, G., Worsnop, D., and O'Dowd, C.: On the effect of wind speed on submicron sea salt mass concentrations and source fluxes, Journal of Geophysical Research-Atmospheres, 117, 10.1029/2011JD017379, 2012.

Paulot, F., Paynter, D., Winton, M., Ginoux, P., Zhao, M., and Horowitz, L.: Revisiting the Impact of Sea Salt on Climate Sensitivity, Geophysical Research Letters, 47, 10.1029/2019GL085601, 2020.

Pennypacker, S. and Wood, R.: A Case Study in Low Aerosol Number Concentrations Over the Eastern North Atlantic: Implications for Pristine Conditions in the Remote Marine Boundary Layer, Journal of Geophysical Research-Atmospheres, 122, 12393-12415, 10.1002/2017JD027493, 2017.

Pennypacker, S., Diamond, M., and Wood, R.: Ultra-clean and smoky marine boundary layers frequently occur in the same season over the southeast Atlantic, Atmospheric Chemistry and Physics, 20, 2341-2351, 10.5194/acp-20-2341-2020, 2020.

Prather, K., Bertram, T., Grassian, V., Deane, G., Stokes, M., DeMott, P., Aluwihare, L., Palenik, B., Azam, F., Seinfeld, J., Moffet, R., Molina, M., Cappa, C., Geiger, F., Roberts, G., Russell, L., Ault, A., Baltrusaitis, J., Collins, D., Corrigan, C., Cuadra-Rodriguez, L., Ebben, C., Forestieri, S., Guasco, T., Hersey, S., Kim, M., Lambert, W., Modini, R., Mui, W., Pedler, B., Ruppel, M., Ryder, O., Schoepp, N., Sullivan, R., and Zhao, D.: Bringing the ocean into the laboratory to probe the chemical complexity of sea spray aerosol, Proceedings of the National Academy of Sciences of the United States of America, 110, 7550-7555, 10.1073/pnas.1300262110, 2013.

Quinn, P., Coffman, D., Johnson, J., Upchurch, L., and Bates, T.: Small fraction of marine cloud condensation nuclei made up of sea spray aerosol, Nature Geoscience, 10, 674-+, 10.1038/NGEO3003, 2017.

Quinn, P., Coffman, D., Kapustin, V., Bates, T., and Covert, D.: Aerosol optical properties in the marine boundary layer during the First Aerosol Characterization Experiment (ACE 1) and the underlying chemical and physical aerosol properties, Journal of Geophysical Research-Atmospheres, 103, 16547-16563, 10.1029/97JD02345, 1998.

Randles, C., Russell, L., and Ramaswamy, V.: Hygroscopic and optical properties of organic sea salt aerosol and consequences for climate forcing, Geophysical Research Letters, 31, 10.1029/2004GL020628, 2004.

Russell, L., Huebert, B., Flagan, R., and Seinfeld, J.: Characterization of submicron aerosol size distributions from time-resolved measurements in the Atlantic Stratocumulus Transition Experiment Marine Aerosol and Gas Exchange, Journal of Geophysical Research-Atmospheres, 101, 4469-4478, 10.1029/95JD01372, 1996a.

Russell, L., Hawkins, L., Frossard, A., Quinn, P., and Bates, T.: Carbohydrate-like composition of submicron atmospheric particles and their production from ocean bubble bursting, Proceedings of the National Academy of Sciences of the United States of America, 107, 6652-6657, 10.1073/pnas.0908905107, 2010.

Russell, L., Zhang, S., Flagan, R., Seinfeld, J., Stolzenburg, M., and Caldow, R.: Radially classified aerosol detector for aircraft-based submicron aerosol measurements, Journal of Atmospheric and Oceanic Technology, 13, 598-609, 10.1175/1520-0426(1996)013<0598:RCADFA>2.0.CO;2, 1996b.

Saliba, G., Chen, C., Lewis, S., Russell, L., Rivellini, L., Lee, A., Quinn, P., Bates, T., Haentjens, N., Boss, E., Karp-Boss, L., Baetge, N., Carlson, C., and Behrenfeld, M.: Factors driving the seasonal and hourly variability of sea-spray aerosol number in the North Atlantic, Proceedings of the National Academy of Sciences of the United States of America, 116, 20309-20314, 10.1073/pnas.1907574116, 2019.

Saliba, G., Chen, C., Lewis, S., Russell, L., Quinn, P., Bates, T., Bell, T., Lawler, M., Saltzman, E., Sanchez, K., Moore, R., Shook, M., Rivellini, L., Lee, A., Baetge, N., Carlson, C., and Behrenfeld, M.: Seasonal Differences and Variability of Concentrations, Chemical Composition, and Cloud Condensation Nuclei of Marine Aerosol Over the North Atlantic, Journal of Geophysical Research-Atmospheres, 125, 10.1029/2020JD033145, 2020.

Salter, M., Nilsson, E., Butcher, A., and Bilde, M.: On the seawater temperature dependence of the sea spray aerosol generated by a continuous plunging jet, Journal of Geophysical Research-Atmospheres, 119, 9052-9072, 10.1002/2013JD021376, 2014.

Salter, M., Zieger, P., Navarro, J., Grythe, H., Kirkevag, A., Rosati, B., Riipinen, I., and Nilsson, E.: An empirically derived inorganic sea spray source function incorporating sea surface temperature, Atmospheric Chemistry and Physics, 15, 11047-11066, 10.5194/acp-15-11047-2015, 2015.

Sanchez, K., Roberts, G., Saliba, G., Russell, L., Twohy, C., Reeves, M., Humphries, R., Keywood, M., Ward, J., and McRobert, I.: Measurement report: Cloud processes and the transport of biological emissions affect southern ocean particle and cloud condensation nuclei concentrations, Atmospheric Chemistry and Physics, 21, 3427-3446, 10.5194/acp-21-3427-2021, 2021.

Schmale, J., Sharma, S., Decesari, S., Pernov, J., Massling, A., Hansson, H., von Salzen, K., Skov, H., Andrews, E., Quinn, P., Upchurch, L., Eleftheriadis, K., Traversi, R., Gilardoni, S., Mazzola, M., Laing, J., and Hopke, P.: Pan-Arctic seasonal cycles and long-term trends of aerosol properties from 10 observatories, Atmospheric Chemistry and Physics, 22, 3067-3096, 10.5194/acp-22-3067-2022, 2022.

Seinfeld, J. H. and Pandis, S. N.: Atmospheric Chemistry and Physics: From Air Pollution to Climate Change, John Wiley & Sons, New York, USA2006.

Sellegri, K., O'Dowd, C., Yoon, Y., Jennings, S., and de Leeuw, G.: Surfactants and submicron sea spray generation, Journal of Geophysical Research-Atmospheres, 111, 10.1029/2005JD006658, 2006.

Shen, Y., Virkkula, A., Ding, A., Luoma, K., Keskinen, H., Aalto, P., Chi, X., Qi, X., Nie, W., Huang, X., Petaja, T., Kulmala, M., and Kerminen, V.: Estimating cloud condensation nuclei number concentrations using aerosol optical properties: role of particle number size distribution and parameterization, Atmospheric Chemistry and Physics, 19, 15483-15502, 10.5194/acp-19-15483-2019, 2019.

Swap, R., Garstang, M., Macko, S., Tyson, P., Maenhaut, W., Artaxo, P., Kallberg, P., and Talbot, R.: The long-range transport of southern African aerosols the tropical South Atlantic, Journal of Geophysical Research-Atmospheres, 101, 23777-23791, 10.1029/95JD01049, 1996.

Tang, I., Tridico, A., and Fung, K.: Thermodynamic and optical properties of sea salt aerosols, Journal of Geophysical Research-Atmospheres, 102, 23269-23275, 10.1029/97JD01806, 1997.

Testa, B., Hill, T., Marsden, N., Barry, K., Hume, C., Bian, Q., Uetake, J., Hare, H., Perkins, R., Mohler, O., Kreidenweis, S., and DeMott, P.: Ice Nucleating Particle Connections to Regional Argentinian Land Surface Emissions and Weather During the Cloud, Aerosol, and Complex Terrain Interactions Experiment, Journal of Geophysical Research-Atmospheres, 126, 10.1029/2021JD035186, 2021.

Uin, J.: Ultra-High Sensitivity Aerosol Spectrometer (UHSAS) instrument handbook., 17, https://doi.org/10.2172/1251410, 2016.

Uin, J., Aiken, A., Dubey, M., Kuang, C., Pekour, M., Salwen, C., Sedlacek, A., Senum, G., Smith, S., Wang, J., Watson, T., and Springston, S.: Atmospheric Radiation Measurement (ARM) Aerosol Observing Systems (AOS) for Surface-Based In Situ Atmospheric Aerosol and Trace Gas Measurements, Journal of Atmospheric and Oceanic Technology, 36, 2429-2447, 10.1175/JTECH-D-19-0077.1, 2019.

Veselovskii, I., Kolgotin, A., Griaznov, V., Muller, D., Wandinger, U., and Whiteman, D.: Inversion with regularization for the retrieval of tropospheric aerosol parameters from multiwavelength lidar sounding, Applied Optics, 41, 3685-3699, 10.1364/AO.41.003685, 2002.

Virkkula, A., Teinila, K., Hillamo, R., Kerminen, V., Saarikoski, S., Aurela, M., Viidanoja, J., Paatero, J., Koponen, I., and Kulmala, M.: Chemical composition of boundary layer aerosol over the Atlantic Ocean and at an Antarctic site, Atmospheric Chemistry and Physics, 6, 3407-3421, 10.5194/acp-6-3407-2006, 2006.

Viskari, T., Asmi, E., Virkkula, A., Kolmonen, P., Petaja, T., and Jarvinen, H.: Estimation of aerosol particle number distribution with Kalman Filtering - Part 2: Simultaneous use of DMPS, APS and nephelometer measurements, Atmospheric Chemistry and Physics, 12, 11781-11793, 10.5194/acp-12-11781-2012, 2012.

von der Weiden, S., Drewnick, F., and Borrmann, S.: Particle Loss Calculator - a new software tool for the assessment of the performance of aerosol inlet systems, Atmospheric Measurement Techniques, 2, 479-494, 10.5194/amt-2-479-2009, 2009.

Von Hoyningen-Huene, W., Dinter, T., Kokhanovsky, A., Burrows, J., Wendisch, M., Bierwirth, E., Muller, D., and Diouri, M.: Measurements of desert dust optical characteristics at Porte au Sahara during SAMUM, Tellus Series B-Chemical and Physical Meteorology, 61, 206-215, 10.1111/j.1600-0889.2008.00405.x, 2009.

Wang, W. and Rood, M.: Real refractive index: Dependence on relative humidity and solute composition with relevancy to atmospheric aerosol particles, Journal of Geophysical Research-Atmospheres, 113, 10.1029/2008JD010165, 2008.

Yu, Q., Zhang, F., Li, J., and Zhang, J.: Analysis of sea-salt aerosol size distributions in radiative transfer, Journal of Aerosol Science, 129, 71-86, 10.1016/j.jaerosci.2018.11.014, 2019.

Zabori, J., Matisans, M., Krejci, R., Nilsson, E., and Strom, J.: Artificial primary marine aerosol production: a laboratory study with varying water temperature, salinity, and succinic acid concentration, Atmospheric Chemistry and Physics, 12, 10709-10724, 10.5194/acp-12-10709-2012, 2012.

Zhang, J. and Zuidema, P.: The diurnal cycle of the smoky marine boundary layer observed during August in the remote southeast Atlantic, Atmospheric Chemistry and Physics, 19, 14493-14516, 10.5194/acp-19-14493-2019, 2019.

Zheng, G., Wang, Y., Aiken, A., Gallo, F., Jensen, M., Kollias, P., Kuang, C., Luke, E., Springston, S., Uin, J., Wood, R., and Wang, J.: Marine boundary layer aerosol in the eastern North Atlantic: seasonal variations and key controlling processes, Atmospheric Chemistry and Physics, 18, 17615-17635, 10.5194/acp-18-17615-2018, 2018.

Zheng, G., Wang, Y., Wood, R., Jensen, M., Kuang, C., McCoy, I., Matthews, A., Mei, F., Tomlinson, J., Shilling, J., Zawadowicz, M., Crosbie, E., Moore, R., Ziemba, L., Andreae, M., and Wang, J.: New particle formation in the remote marine boundary layer, Nature Communications, 12, 10.1038/s41467-020-20773-1, 2021.

Zieger, P., Fierz-Schmidhauser, R., Gysel, M., Strom, J., Henne, S., Yttri, K., Baltensperger, U., and Weingartner, E.: Effects of relative humidity on aerosol light scattering in the Arctic, Atmospheric Chemistry and Physics, 10, 3875-3890, 10.5194/acp-10-3875-2010, 2010.

Zuidema, P., Redemann, J., Haywood, J., Wood, R., Piketh, S., Hipondoka, M., and Formenti, P.: Smoke and Clouds above the Southeast Atlantic Upcoming Field Campaigns Probe Absorbing Aerosol's Impact on Climate, Bulletin of the American Meteorological Society, 97, 1131-1135, 10.1175/BAMS-D-15-00082.1, 2016.

Table 1. LASIC measurements analyzed in this study.

Variable	instrument	measurement	temporal resolution	measured relative humidity (RH) (%)	availability[a]	data access
Particle Size Distributions						
	Ultra-High Sensitivity Aerosol Spectrometer (UHSAS)	dry particle size distributions D_p: 0.06 – 1 µm (optical diameter)	1 Hz	55 ± 8[b]	2016 Nov. – 2017 May	https://doi.org/10.5439/1333828
	Scanning Mobility Particle Sizer (SMPS)	dry particle size distributions D_p: 0.01 – 0.46 µm (mobility diameter)	5 min	55 ± 8[b]	2016 Nov – 2017 May	https://doi.org/10.5439/1225453
Particle Scattering						
	TSI 3563 3-wavelength Integrating Nephelometer (NEPH)	< 1 µm and < 10 µm dry total scattering coefficients at 450, 550, and 700 nm wavelengths	1 min (alternating impactor size cuts approximately every 55 min)	60 ± 4[c]	2016 Nov. – 2017 May	https://doi.org/10.5439/1259232
Ancillary						
	Aerodyne Research Aerosol Chemical Speciation	mass concentration of non-refractory submicron	15 min		2017 Jan. – 2017 May	https://doi.org/10.5439/1762267

Deleted: [1]

Formatted Table

Deleted: 60

Deleted: cutoff

Monitor (ACSM)	chloride aerosol				
TSI Ultrafine Condensation Particle Counter 3776	condensation nuclei concentration of particles > 3 nm	1 min		2016 Nov. – 2017 May	https://doi.org/10.5439/1046186
Vaisala WXT-520	wind speed and rain intensity	1 min		2016 Nov. – 2017 May	https://doi.org/10.5439/1025153
DMT Single Particle Soot Photometer	refractory black carbon concentration	15 min		2016 Nov. – 2017 May	https://iop.archive.arm.gov/arm-iop/2016/asi/lasic/sedlacek-sp2/
Los Gatos Research trace gas analyzer	carbon monoxide mixing ratio	1 min		2016 Nov. – 2017 May	https://doi.org/10.5439/1046183
Radiance Research Particle Soot Absorption Photometer (PSAP)	< 1 µm and < 10 µm dry total absorption coefficients at 470, 552, and 660 nm wavelengths	1 min	< 25%	2016 Nov. – 2017 May	https://doi.org/10.5439/1339528

[a]full availability defined as typical Ascension Island background season (November – May).

[b]Not reported in dataset. Estimated from internal temperature, ambient temperature, and ambient RH.

[c]Nephelometer measurements used for retrieval were restricted to periods when the RH was below 60% (Section 2.1.2).

Deleted: [1]

Deleted: during

Table 2. Scattering and size distribution measurements and the associated uncertainties and variabilities used in the sea spray mode retrieval method.

Measurement			Variability or Uncertainty		
Scattering					Range /Selected Value
	$b_{sca,1\text{-}10\mu m}(\lambda)$	supermicron scattering at red (700 nm), green (550 nm), and blue (450 nm) light wavelengths	$\sigma_{sca,1\text{-}10\mu m}(\lambda)$	standard deviation of supermicron scattering for averaging time at each wavelength	0.4 – 40.0 Mm^{-1}
			$\sigma_{sca,inst}$	instrument-defined scattering uncertainty	5%
Size Distribution					
	PNSD	particle number size distribution	$\sigma_{PNSD,meas}(D_p)$	standard deviation of PNSD resolved at each size bin	0.01 – 300 cm^{-3}
			$\sigma_{PNSD,inst}$	instrument-defined concentration uncertainty	10%
	D_p	PNSD diameters	σ_D	instrument-defined sizing uncertainty	2.5%

Deleted: (5%)

Deleted: (10%)¶

Deleted: (2.5%)

Table 3. Lognormal mode fitting parameters and resolution (step) used to derive Mie scattering sea spray mode solutions.

Parameter	unit	minimum value	maximum value	step
N_t	cm^{-3}	1.0	99	2.0
D_g	µm	0.05	1.19	0.015
σ_g		1.0	4.0	0.075

Table 4. Comparison of retrieved sea spray modal parameters using measured supermicron size distributions (SEMS-APS; Saliba et al., 2019) and Mie inversion of nephelometer supermicron scattering (SEMS-NEPH; this study) during clean marine periods of the NAAMES 1 cruise (6 November – 30 November 2015). Values of the 2-h integrated number (N_T) concentration, mass concentration (M_T), number mean diameter ($D_{g,number}$), mass mean diameter ($D_{g,mass}$) and mode width (σ_g) are provided as the mean ± 1 standard deviation.

	N_T (cm^{-3})	M_T ($\mu g\ m^{-3}$)	$D_{g,number}$ (μm)	$D_{g,mass}$ (μm)	σ_g
SEMS-NEPH	7.1 ± 2.1	6.1 ± 2.7	0.6 ± 0.1	1.1 ± 0.3	2.0 ± 0.3
SEMS-APS	4.2 ± 3.4	5.5 ± 3.4	0.5 ± 0.2	1.5 ± 0.3	2.4 ± 0.3

Table 5. UHSAS-only and UHSAS-NEPH number concentrations, mass concentrations, and size distribution fitting parameters. Values are mean ± 1 standard deviation. Bracketed values are the minimum and maximum ranges.

	UHSAS-only	UHSAS-NEPH
N_T (cm^{-3})	8 ± 7	6 ± 3
	[0, 151]	[0, 34]
M_T ($\mu g\ m^{-3}$)	1.3 ± 2.2	8.37 ± 4.1
	[0.008, 23.5]	[0.18, 23.0]
$D_{g,number}$ (µm)	0.42 ± 0.10	0.51 ± 0.10
	[0.050, 0.54]	[0.16, 1.0]
$D_{g,mass}$ (µm)	0.68 ± 0.01	1.47 ± 0.17
	[0.4, 1.6]	[0.6, 1.9]
σ_g	1.8 ± 0.4	2.4 ± 0.3
	[1.3, 5.3]	[1.1, 3.97]

Deleted: 4
Deleted: 4
Deleted: 47
Deleted: 8
Deleted: 7
Deleted: 6.6
Deleted: 3.5
Deleted: 42
Deleted: 3
Deleted: 0
Deleted: 7
Deleted: 49
Deleted: 0
Deleted: 0.89
Deleted: 1.3
Deleted: 0.15
Deleted: 6
Deleted: 2
Deleted: 2
Deleted: 2

Table 6. Literature reported values of sea spray modal parameters. Number mean diameters ($D_{g,number}$) were converted to mass mean diameters ($D_{g,mass}$) using Eq. (7), integrating over particle sizes 0.01 – 10 µm, and averaging over a total particle concentration range of 1 – 100 cm^{-3}. Values are averages unless noted as an upper or lower bound.

Deleted: 5

			Parameter		
Reference	**Experiment type**	**Ocean basin**	**$D_{g,number}$ (µm)**	**$D_{g,mass}$ (µm)**	**σ_g**
Lewis and Schwartz (2004), Sellegri et al. (2006), Keene et al. (2007), Fuentes et al. (2010), Modini et al. (2010), Bates et al. (2012), Zabori et al. (2012)	field measurements (RH: 80%)		0.3	1.3	3
	laboratory-based bubble bursting (RH: variable)		0.05 (lower bound) 0.1 (upper bound)	0.25 (lower bound) 0.48 (upper bound)	2.8
Prather et al. (2013)	laboratory-based breaking wave flume (RH: 10 ± 15%)	N.E. Pacific	0.16	0.88	3
Modini et al. (2015)	field measurements (RH: < 40%)	N.E. Pacific	0.14 (lower bound) 0.26 (upper bound)	0.5 (lower bound) 1.3 (upper bound)	2.5 (lower bound) 3 (upper bound)
Quinn et al. (2017)	field measurements (RH: variable, mostly ≤ 50%)	Pacific, Southern, Arctic, and Atlantic	0.3	1.08	2.5
Saliba et al. (2019)	field measurements (RH: < 40%)	N. Atlantic	0.5	1.6	2.3
Sanchez et al.	field measurements	Southern Ocean	0.6	0.71	1.4

(2021)	(RH: ambient)				
This study	field measurements (RH = 55 ± 10%)	S. Atlantic	0.4 (UHSAS-only) 0.5 (UHSAS-NEPH)	0.68 (UHSAS-only) 1.47 (UHSAS-NEPH)	1.8 (UHSAS-only) 2.4 (UHSAS-NEPH)

Deleted: 3

Deleted: 2

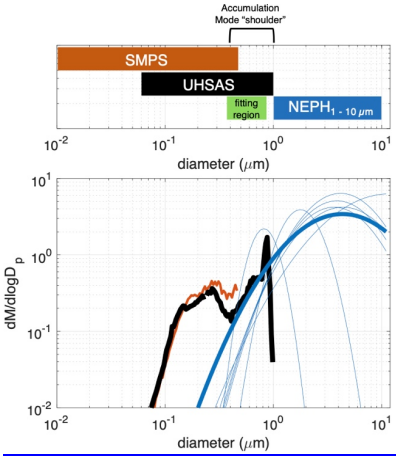

Figure 1. Schematic demonstrating the sea spray mode retrieval method using Mie theory-simulated size distributions, 3-wavelength integrating nephelometer supermicron scattering measurements, and UHSAS submicron mass size distributions (UHSAS-NEPH). The retrieval shown is for a 2-h averaging period beginning 29 November 2016 14:00 UTC. (top panel) Instrument size ranges and mode fitting region for size distributions. (bottom panel) Mass size distributions (μg m^{-3}) measured by the SMPS (orange) and UHSAS (black), probable Mie theory-simulated lognormal sea spray mode solutions (thin blue), and best constrained Mie solution (thick blue). Note the UHSAS instrument artifact at D_p = 0.85 μm (see text for description).

Deleted: r

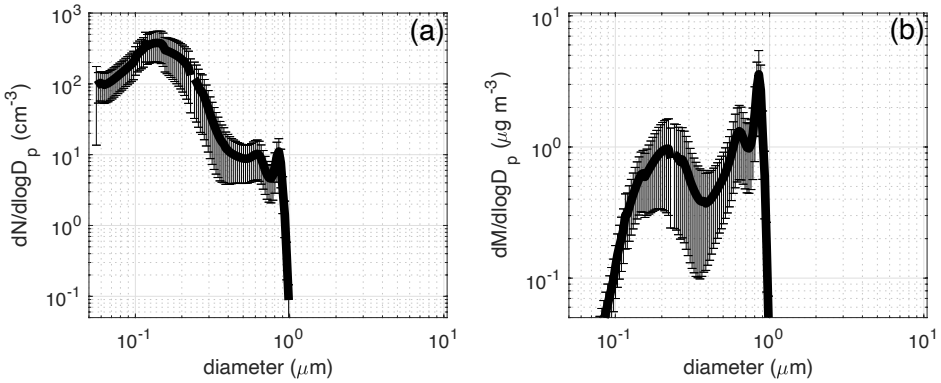

Figure 2. Average (solid black line) and variability (1 standard deviation; error bars) of the UHSAS (a) number (cm^{-3}) and (b) mass (μg m^{-3}) size distributions during the clean marine background season of LASIC (November 2016 – May 2017).

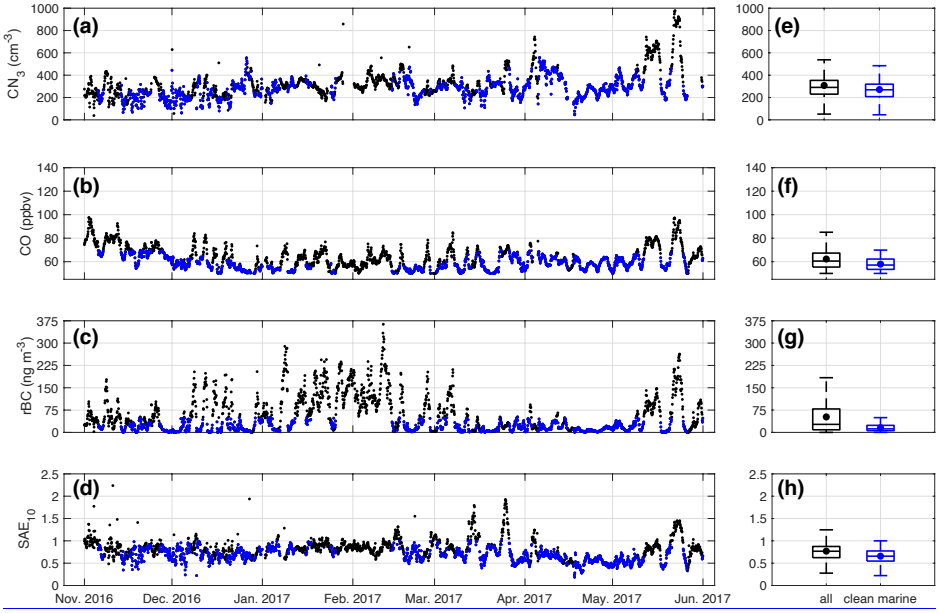

Figure 3. Time series (a-d) and box-and-whisker plots (e-h) of 2-h average variables used to determine clean marine periods during the LASIC background season (November 2016 – May 2017). (a-d) Periods that meet the criteria thresholds described in Section 2.2 are symbolized by blue dots. (e-h) Circles within the box-and-whisker plots are the means and horizontal lines are the median and interquartile ranges (25% and 75%) for the background season (black) and clean marine periods (blue).

Deleted:

Deleted:

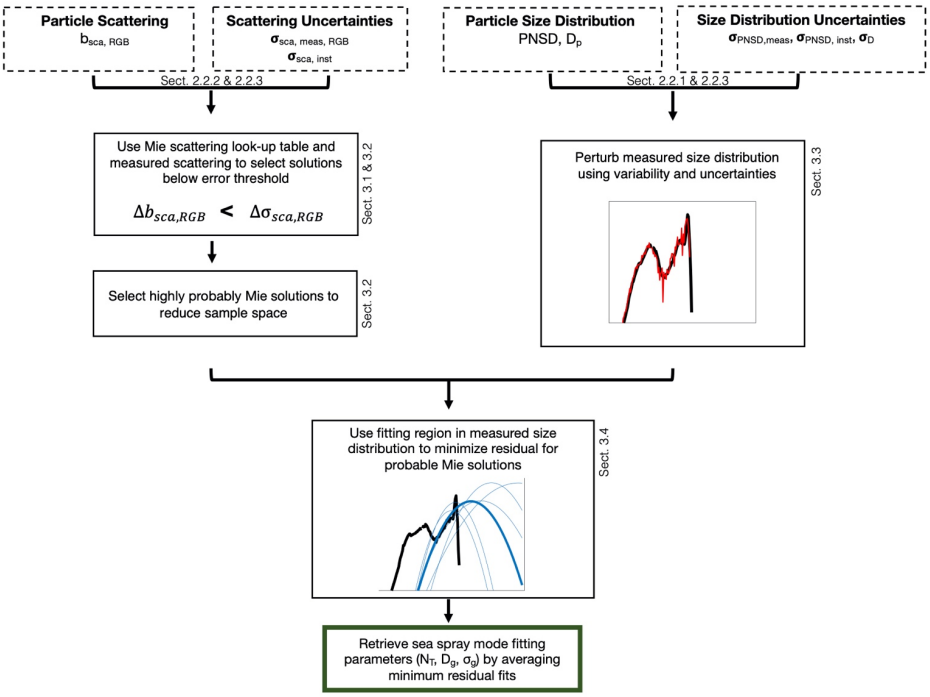

Figure 4. Flow chart describing the UHSAS-NEPH retrieval algorithm. Direction to descriptive procedures of each step are identified by main text section at right (below) the boxes.

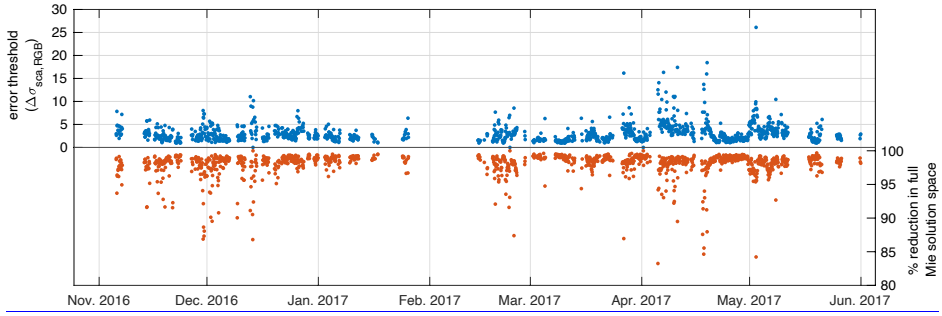

Figure 5. (top, blue) Time series of the scattering error threshold ($\Delta\sigma_{sca,RGB}$, Mm^{-1}) and (bottom, orange) percent reduction of the Mie look-up table solution space (N = 157,850) for UHSAS-NEPH retrievals during the background season of LASIC.

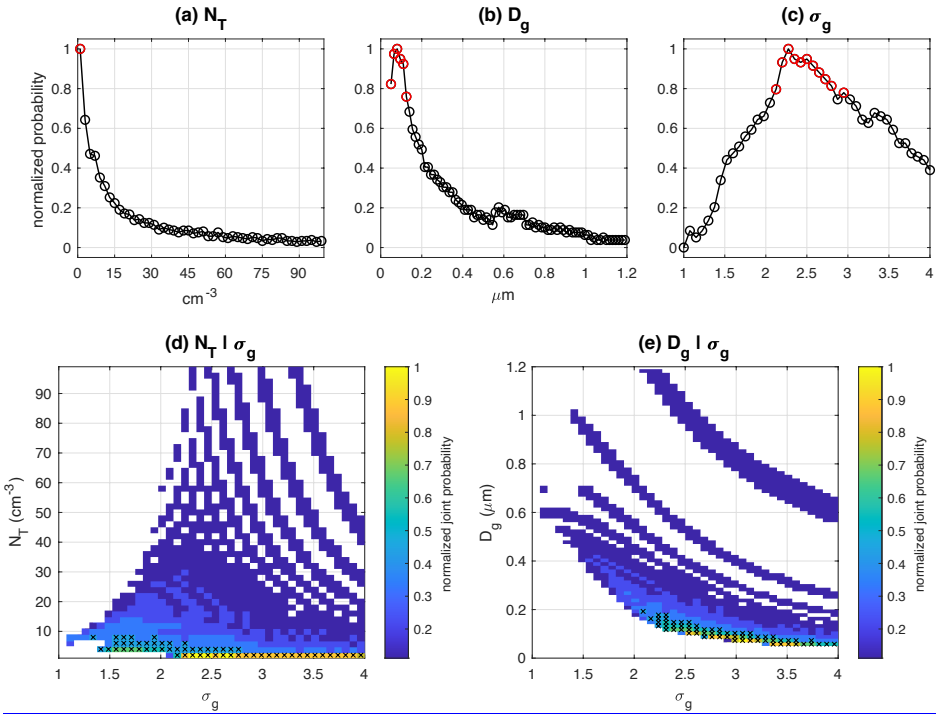

Figure 6. (a-c) Normalized probability distributions of sea spray mode fitting parameters obtained for one retrieval (3 December 2016 22:00 UTC). (a-c) Fitting parameter values with an occurrence probability of greater than 75% are symbolized by red circles. (d-e) Normalized joint probabilities (color bar) for fitting parameter combinations of $N_T \mid \sigma_g$ and $D_g \mid \sigma_g$ from the same retrieval. Mie solutions that are within the top 5th joint probability percentile for each combination are symbolized by black crosses.

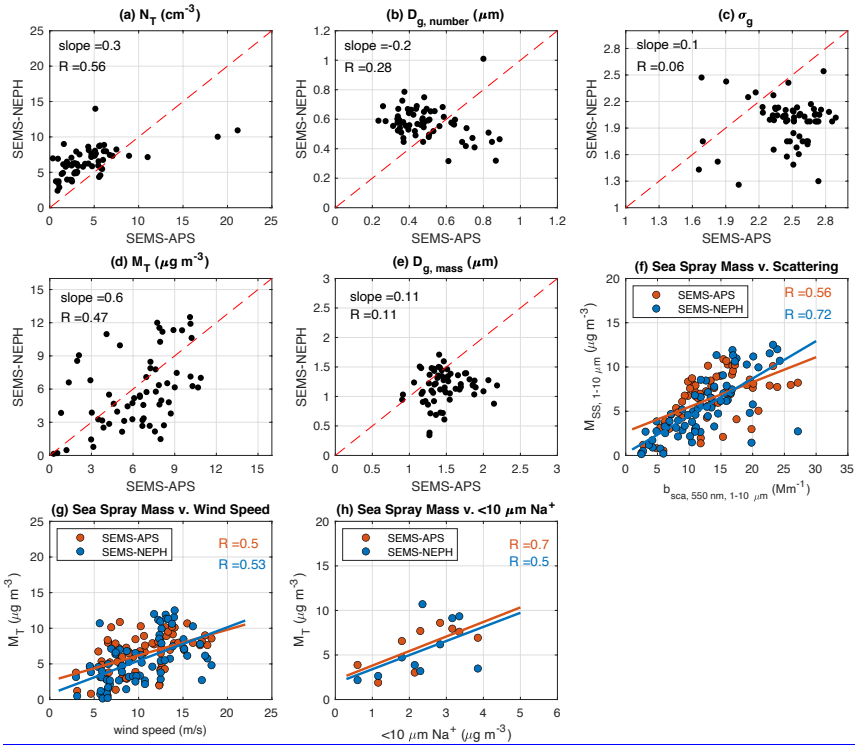

Figure 7. Comparison of retrieved sea spray modal parameters using measured supermicron size distributions (SEMS-APS; Saliba et al., 2019) and Mie inversion of nephelometer supermicron scattering (SEMS-NEPH; this study) during clean marine periods of the NAAMES 1 cruise (6 November – 30 November 2015). 2-h integrated (a) number (cm^{-3}) and (d) mass ($\mu g\ m^{-3}$) concentrations, (b) number and (e) mass mean diameters (μm), and (c) mode width. (a-e) Slope of linear best fit and Pearson correlation coefficients at top left. Dashed red lines represent a 1:1 line. Sea spray mass correlation with supermicron scattering (f), wind speed (g), and < 10 μm Na^+ mass concentration (h) for SEMS-APS (orange) and SEMS-NEPH (blue) methods. Na^+ mass measurements are from offline filter analysis using ion chromatography. Sea spray mass estimates in (h) are averaged over the filter collection times (24-h) which provided 9 samples. Pearson correlation coefficients indicated at top right and linear best fit colored by method in (f,g,h).

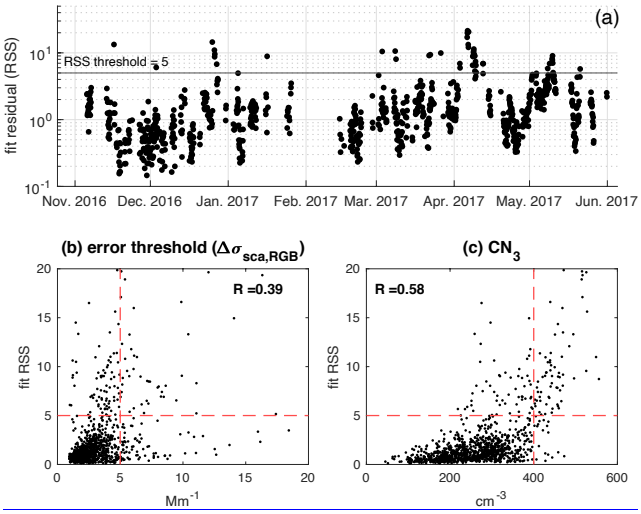

Figure 8. (a) Times series of the fit residual (residual sum of squares, RSS) between the retrieved sea spray mode and UHSAS mass size distribution within the 0.38 – 0.83 µm fitting region. The horizontal line in (a) delineates an RSS restriction threshold of 5 used in this procedure. Note logarithmic y-axis. (b,c) Selected variables used to restrict sea spray mode retrievals defined by the fit residual (fit RSS, y-axes). (b) error threshold ($\Delta\sigma_{sca,RGB}$, Mm^{-1}) and (c) condensation nuclei concentration of particles > 3 nm optical diameter (cm^{-3}). Retrieval restriction thresholds are symbolized by dashed red lines in (b,c). Pearson correlation coefficients ($p < 0.05$) are provided within panels (b,c).

Deleted: 6

Deleted: H

Deleted: -

Deleted: d

Deleted: , (c) relative humidity within the nephelometer (%),

Deleted: d

Deleted: hin each

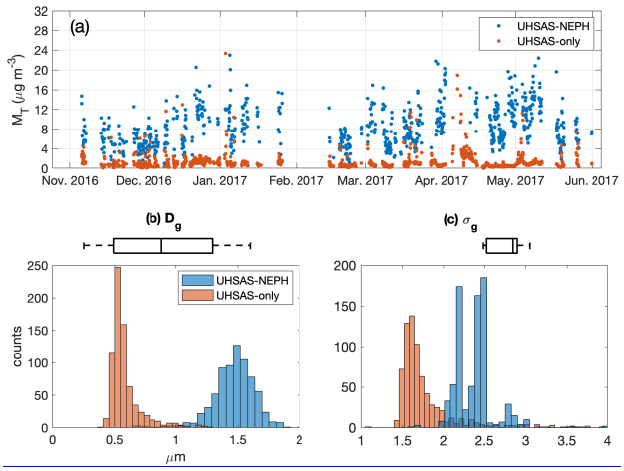

Figure 9. (a) Time series of sea spray mass concentration (M_T, µg m^{-3}) retrieved from UHSAS-NEPH (blue) and UHSAS-only (orange) during clean marine periods of the LASIC background season (see Table 5 for summary statistics). Histograms of the (b) geometric mean mass diameter (D_g) and (c) geometric standard deviation (σ_g mode width) for the retrieved sea spray modes using UHSAS-NEPH and UHSAS-only. Box-and-whisker plots above the histograms represent the quartile ranges (25th and 75th) and median (vertical line) of sea spray mode fitting parameters reported in laboratory and field measurements (see Table 6).

Deleted: 7

Deleted: ss

Deleted: 4

Deleted: 5

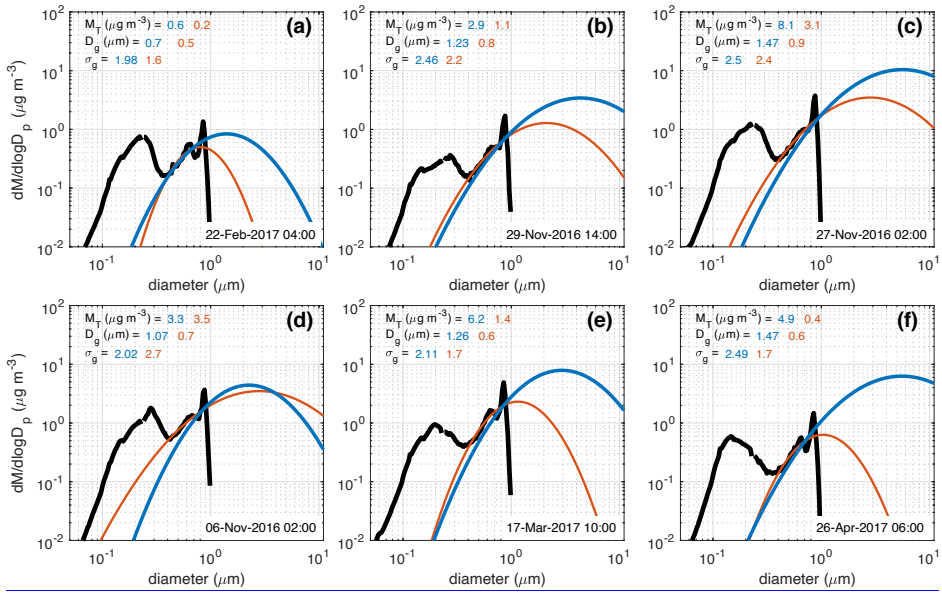

Figure 10, Selected characteristic fits to the sea spray mode. UHSAS mass size distribution (black), UHSAS-NEPH (blue), and UHSAS-only (orange). Panels are oriented to reflect increasing mass, size, and width of the sea spray mode retrieved by UHSAS-NEPH from left to right (a-c, d-f). Mode fitting parameters for the UHSAS-NEPH and UHSAS-only methods are identified in text and specified by method color within each panel: total mode mass (M_T), geometric mean mass diameter (D_g), and geometric standard deviation (σ_g). 2-h average time stamps are provided at the lower right.

Deleted: 8

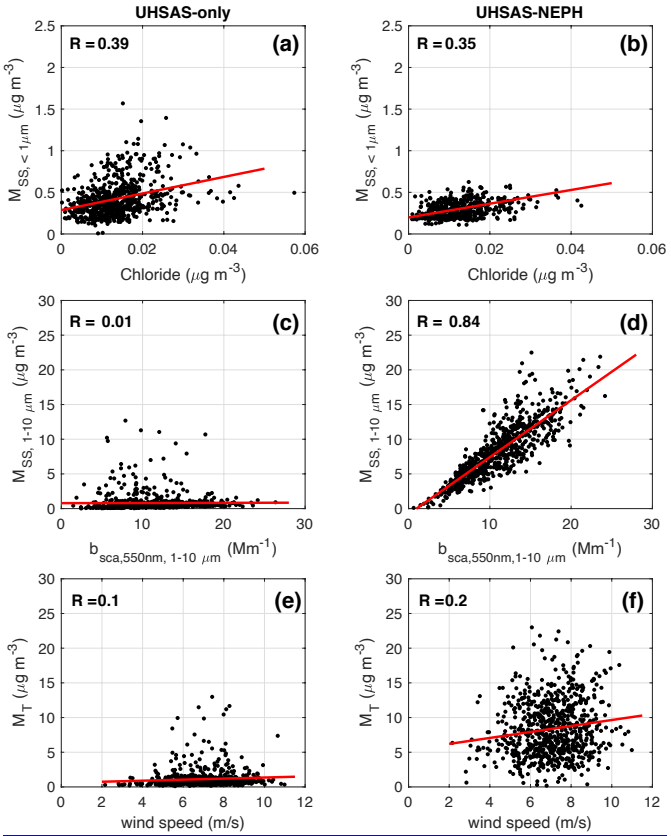

Figure 11. Correlations of submicron sea spray mass ($M_{SS,<1\mu m}$; μg m^{-3}) with ACSM chloride (a,b), supermicron sea spray mass ($M_{SS,1\text{-}10\mu m}$; μg m^{-3}) and measured supermicron scattering at 550 nm (c,d), total sea spray mode mass (M_T, μg m^{-3}) with wind speed (e,f) for UHSAS-only (left) and UHSAS-NEPH (right) methods. Linear regressions are symbolized by red lines and correlation coefficients are provided inside of the panels.

Deleted: 9